SANDIA REPORT

SAND99–0975
Unlimited Release
Printed April 1999

Reliability Degradation Due to Stockpile Aging

David G. Robinson

Prepared by
Sandia National Laboratories
Albuquerque, New Mexico 87185 and Livermore, California 94550

Sandia is a multiprogram laboratory operated by Sandia Corporation, a Lockheed Martin Company, for the United States Department of Energy under Contract DE-AC04-94AL85000.

Sandia National Laboratories

Issued by Sandia National Laboratories, operated for the United States Depart-ment of Energy by Sandia Corporation.

Available to DOE and DOE contractors from
Office of Scientific and Technical Information
P.O. Box 62
Oak Ridge, TN 37831

Prices available from (703) 605-6000
Web site: http://www.ntis.gov/ordering.htm

Available to the public from
National Technical Information Service
U.S. Department of Commerce
5285 Port Royal Rd
Springfield, VA 22161

NTIS price codes
Printed copy: A03
Microfiche copy: A01

DISCLAIMER

Portions of this document may be illegible in electronic image products. Images are produced from the best available original document.

SAND 99-0975
Unlimited Release
Printed April 1999

Reliability Degradation Due to Stockpile Aging

David G. Robinson
Systems Reliability
Sandia National Laboratories
P.O. Box 5800
Albuquerque, NM 87185-0746

drobin@sandia.gov

Abstract

The objective of this research is the investigation of alternative methods for characterizing the reliability of systems with time dependent failure modes associated with stockpile aging. Reference to 'reliability degradation' has, unfortunately, come to be associated with all types of aging analyses: both deterministic and stochastic. In this research, in keeping with the true theoretical definition, reliability is defined as a probabilistic description of system performance as a function of time. Traditional reliability methods used to characterize stockpile reliability depend on the collection of a large number of samples or observations. Clearly, after the experiments have been performed and the data has been collected, critical performance problems can be identified. A major goal of this research is to identify existing methods and/or develop new mathematical techniques and computer analysis tools to anticipate stockpile problems before they become critical issues. One of the most popular methods for characterizing the reliability of components, particularly electronic components, assumes that failures occur in a completely random fashion, i.e. uniformly across time. This method is based primarily on the use of constant failure rates for the various elements that constitute the weapon system, i.e. the systems do not degrade while in storage. Experience has shown that predictions based upon this approach should be regarded with great skepticism since the relationship between the life predicted and the observed life has been difficult to validate. In addition to this fundamental problem, the approach does not recognize that there are time dependent material properties and variations associated with the manufacturing process and the operational environment. To appreciate the uncertainties in predicting system reliability a number of alternative methods are explored in this report. All of the methods are very different from those currently used to assess stockpile reliability, but have been used extensively in various forms outside Sandia National Laboratories. It is hoped that this report will encourage the use of 'nontraditional' reliability and uncertainty techniques in gaining insights into stockpile reliability issues.

Contents

Figures

Tables

Reliability Degradation Due to Stockpile Aging

1. Background

1.1 Objective

The objective of the research outlined in this document is the investigation of alternative methods for characterizing the reliability of systems with time dependent failure modes associated with stockpile aging. Traditional reliability methods used to characterize stockpile reliability depend on the collection of a large number of samples or observations. Clearly, after the experiments have been performed and the data has been collected, critical performance problems can be identified. A major goal of this research is to identify existing methods and/or develop new mathematical techniques and computer analysis tools to anticipate stockpile problems before they become critical issues. As depicted in Figure 1.1, by statistically characterizing performance degradation, these techniques provide a means to quantify the probability of poor performance prior to actually degrading to the critical operational condition.

1.2 Contrast with Traditional Methods

One of the most popular methods for characterizing the reliability of components, particularly electronic components, assumes that failures occur in a random fashion. This method is based primarily on the use of constant failure rates for the various elements that constitute the weapon system, i.e. the systems do not degrade while in storage. Experience has shown that predictions

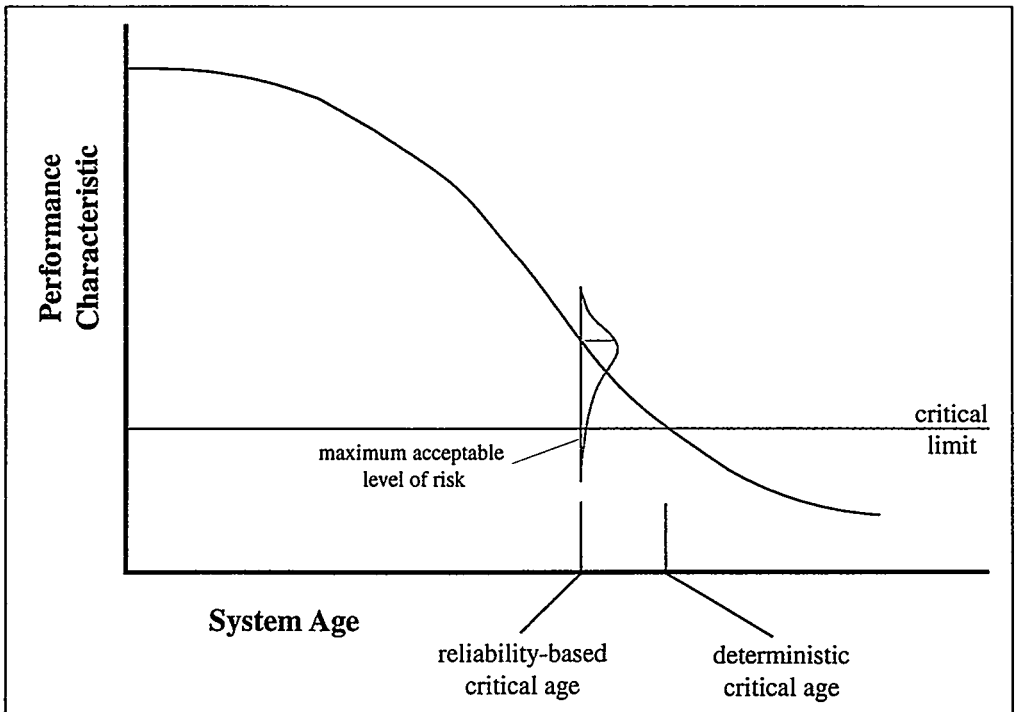

Figure 1.1 Reliability-based versus Deterministic Performance Analysis

based upon this approach should be regarded with great skepticism since the relationship between the life predicted by handbook data and the observed life has been difficult to validate. In addition to this fundamental problem, the approach does not recognize that there are time dependent material properties and also variations associated with the manufacturing process and the operational environment. A very common technique aimed at reducing the error associated with ignoring time dependency is to allow the constant failure rates to be random variables. This only tends to increase the inaccuracy and make the problem more intractable. However, the method does benefit from being extremely easy to use, albeit very inaccurate when dealing with age related reliability problems.

A major source of the error in using these very traditional reliability methods, even time dependent methods, is that all these techniques view system operation as a go/no-go situation. The current practice at many companies is to test a system/subsystem, and, if it is operating within specifications, label the test as a success. No attempt is made to monitor the degradation of the system performance characteristics as a function of system age and relate these observations to storage reliability. The alternative proposed here suggest that by monitoring system performance through testing, in conjunction with science-based modeling, it is possible to characterize time dependent changes in material properties and identify aging related problems earlier, with fewer test resources.

1.3 Incorporating Uncertainty

This research has focused on investigating mathematical methods for incorporating uncertainty in traditional deterministic modeling, in particular, the advanced phenomenological modeling and simulation techniques used to characterize the physics of the underlying failure processes. As depicted in Figure 1.2, uncertainties in these deterministic models naturally arise from a variety of sources:

- model (model is only an abstract representation of reality)
  - modeling approach
  - model fidelity
- model parameters
  - yield strength
  - conductivity
  - chemical composition
  - interaction between dissimilar materials, etc
- input parameters (operating environment)
  - temperature
  - humidity
  - vibration levels
  - voltage, etc.

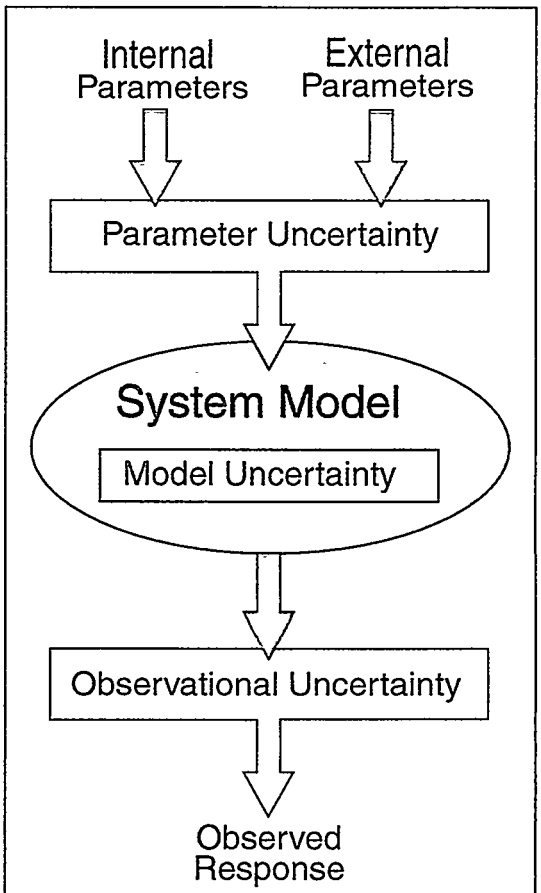

Figure 1.2 Sources of Uncertainty

The above discussion should not be misconstrued as a suggestion that testing and experimentation can be replaced. On the contrary, probabilistic methods provide a means to quantify the potential risk associated with a particular failure mode and can help focus additional testing and experimentation. The result will be a more efficient use of test resources and a more timely attention to critical problems. Figure 1.3 depicts the relationship between testing, modeling and uncertainty/reliability analyses.

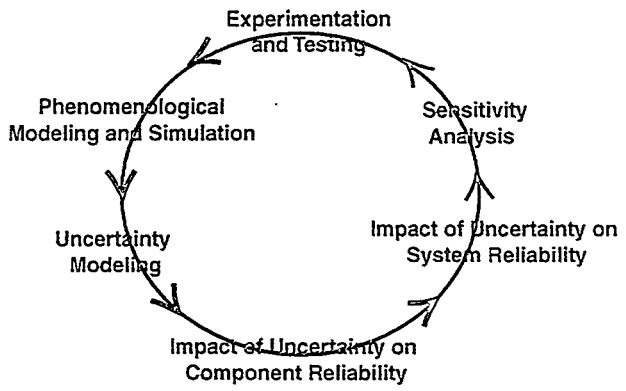

Figure 1.3 Experimentation - Analysis Cycle

This approach permits a more efficient use of limited test resources and also assists design engineers in planning for new materials and manufacturing techniques. This is particularly important as Sandia moves towards commercial off-the-shelf replacement (COTS) components.

For example, the cycles to failure of a leadless surface mounted integrated circuit is commonly characterized by some form of the Coffin-Manson expression:

$$N_f = \frac{1}{2}\left[\frac{\Delta\gamma}{\varepsilon_f}\right]^{\frac{1}{c}} \qquad [1.1]$$

where: c is a known constant, $\Delta\gamma$ is the cyclic shear strain, and ε_f is the fatigue ductility coefficient [Engelmaier, 1991]. In reality the 'constant' c depends on the temperatures of the component, the substrate and the ambient operating environment. The total cyclic strain range $\Delta\gamma$ depends on, among many other factors, the solder joint geometry, distances between solder connections, solder/component material expansion differences and is sensitive to the existence of brittle intermetallic compounds.

This empirical equation and the associated constants are constructed from an initial sequence of controlled experiments; the relationship between the equation, the conditions under which it was developed and what will be experienced under storage conditions is tenuous at best. Variation in any one of these factors can result in significant variation in the estimated fatigue life of the solder connection. However, by recognizing that there is uncertainty in the various model parameters (and perhaps within the model itself), and characterizing that uncertainty in probabilistic terms, it is possible to identify those parameters which should be the focus of future test efforts.

As a second example, consider the well known Arrhenius accelerated aging technique. This method has been popular with materials engineers since the late 1800's. Methods of analysis such as Arrhenius are also considered deterministic, which is to say that once the system has been deployed in its 'isothermal' environment, its lifetime can be determined through calculation. That is, random effects of operating environment, material properties, etc. are considered unimportant.

1.4 Approach

Probabilistic methods are typically applied to address one of two basic questions: What does the probability density function of the system response look like? Or, alternatively: What is the probability that the system response exceeds a critical level? From a reliability engineering design and analysis point of view, the latter approach is the most common since reliability engineers are typically responsible for describing the probability of system failure relative to a set of design codes or specifications. Interest in system response is typically focused on a particular region of interest rather than the entire domain of possible system responses. Further, by examining a number of possible 'critical levels', clearly the density function of the system response can be completely characterized (rather than evaluated at simply one point).

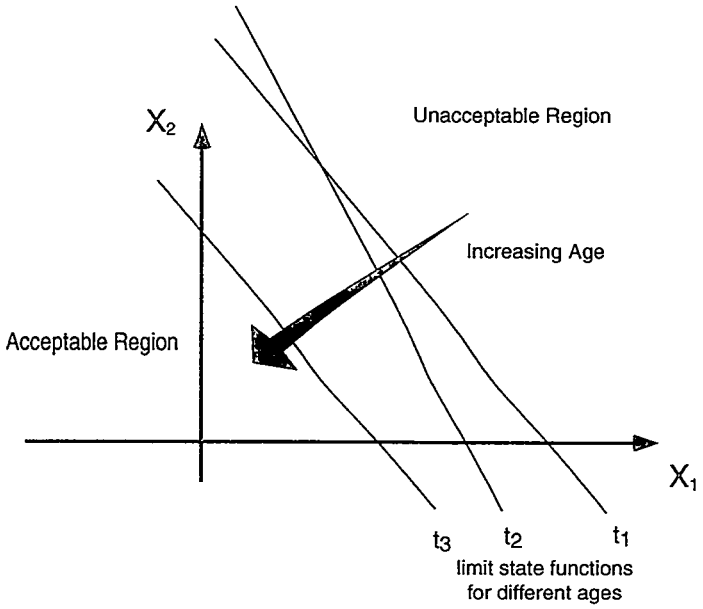

Figure 1.4 Changes in Limit State Description as System Ages

Assuming the existence (real or artificial) of a critical level of system performance, the result is the partitioning of the system parameter domain $\mathbf{x} = (x_1, x_2, \ldots, x_n)$ into two regions: a region Ω where combinations of system parameters lead to an unacceptable or unsafe system response and a safe region $\overline{\Omega}$ where system response is acceptable. The surface dividing these regions is generally referred to as the limit state surface or limit state function. The probability of system failure is then defined by the expression:

$$p_f = \iint \cdots \int_{\Omega} f_{\mathbf{X}}(\mathbf{x}) d\mathbf{x}$$

where $f_{\mathbf{X}}(\mathbf{x})$ is the joint probability density function (pdf). Except for some unique limit state functions and joint density functions (e.g. linear limit state and Gaussian distributed random variables), the integral can be very difficult to evaluate. A variety of methods are available to solve this integral; the correct choice may depend a great deal on the specific problem formulation. A number of methods will be briefly mentioned in the following discussion. For a more complete discussion of the different methods, the reader is referred to a series of survey papers (in various stages of completion) available from the author [Robinson, 1998].

It is important to understand that the approach used in the following analyses assumes that the statistical properties of the underlying aging process are separable from time. That is, it is possible to completely characterize the joint density function $f_{\mathbf{X}}(\mathbf{x})$ at a particular time t_i without knowledge of the density function for all $t \le t_i$. Figures 1.1, 1.4 and 1.5 depict different views of the approach. As in Figure 1.4, we can view the limit state function as changing as the

system ages and the performance degrades. From another perspective, as depicted in Figure 1.5, we can view the statistical characterization of system performance changing as the system ages.

The are many aging problems where this approach provides only an approximate result. However, the applications where there are significant benefits to be gained by a more intensive stochastic analysis are fortunately less frequent. In addition, the advanced methods rely a great deal on the statistical foundation described here. So the discussion here centers on the more fundamental techniques that have a broader range of application.

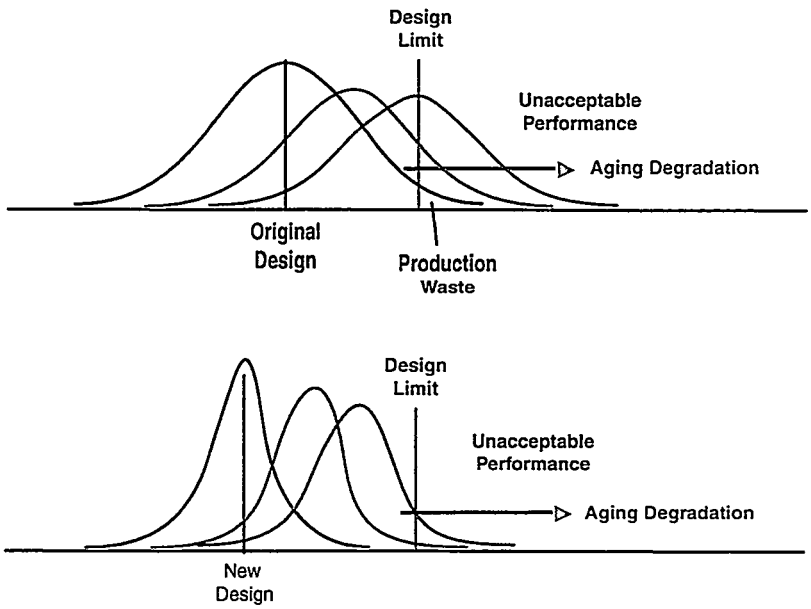

Figure 1.5 Impact of Design Changes on Aging Characteristic

1.5 Notation

The notation used in the following discussion is consistent with the literature; however, it can be confusing to the uninitiated. The following definitions will be consistent throughout.

$\mathbf{x} = \{x_1,\ldots,x_n\}$: a vector of *independent* random variables generally referred to individually as *design* variables. The performance of the system is defined in terms of these variables and the locus of all feasible combinations of these variables is referred to as the *design space*.

$\mathbf{y} = \{y_1,\ldots,y_n\}$: identical to the vector $\mathbf{x}$ with the exception that these random variables are assumed to be *statistically dependent.*

$\mathbf{u} = \{u_1,\ldots,u_n\}$: a vector of statistically independent random variables with zero mean and unit standard deviation.

$G(\mathbf{x}), g(\mathbf{x})$: the performance of the system is assumed to be a function of a set of design variables and is referred to as the *system performance function* or *system response function.* This function may be explicit or implicit.

$\phi(\cdot)$: standard normal density function - $\phi(z) = \frac{1}{\sqrt{2\pi}}\exp\left(-\frac{z^2}{2}\right)$

$\Phi(\cdot)$: cumulative normal density function - $\Phi(z) = \frac{1}{\sqrt{2\pi}}\int_{-\infty}^{z}\exp\left(-\frac{s^2}{2}\right)ds$

limit state function: a set defined by the locus of points: $G(\mathbf{x}) = 0$.

failure region: the limit state function divides the feasible space into (at least) two regions: the failure or unsafe region $G(\mathbf{x}) < 0$ and the safe region: $G(\mathbf{x}) > 0$. These definitions are based on historical convention rather than a specific requirement. The use of the terms 'failure' is also customary, since only the likelihood of a particular system state may be of interest rather than system failure.

safety index: β, the safety index, is defined as the scalar distance, in standard normal space, from the origin to the limit state function. When used in the context of $\Phi(-\beta)$ it is assumed that $\beta > 0$. For a linear limit state function and Gaussian distributed random variables, it can be shown that $\beta = \frac{\mu_G}{\sigma_G}$, the ratio of the mean system response and the standard deviation of the system response (both evaluated at the critical or failure point).

1.6 Summary

In summary, the goal of this research is the investigation into modeling and analysis techniques that will permit: time dependent consideration of uncertainties in material behavior, processes and operating conditions and allow:

- data from a variety of test programs to be incorporated into the analysis
- engineers to identify critical performance parameters that need to be closely monitored and controlled
- stockpile aging problems to be addressed in an anticipatory, coordinated effort rather than waiting for the problem to actually manifest itself.

In the course of the research these techniques have been applied to three major areas of concern in stockpile aging: stress voiding of interconnections in integrated circuits, corrosion of electronic components and accelerated aging analysis of polymers. The applications have been chosen because they demonstrate the wide applicability of the uncertainty methods in aging analysis and were also of current interest in stockpile reliability assessment. Each of these areas is a topic of successive chapters. The emphasis in this report is the discussion of applications. Details on the specific methods that were used is documented in a series of Survey reports [Robinson, 1998]. The final chapter is devoted to a brief discussion of the software tools being developed to assist the design engineers in incorporating reliability and uncertainty methods directly in their analyses.

2. Stress Voiding of Electronic Circuits

2.1 Introduction

This chapter discusses a statistical characterization of the nucleation and subsequent growth of conductor line voids due to stress-induced mass diffusion. Experience has shown that even without a voltage load (e.g. storage conditions), voids appear and propagate in the thin aluminum films used in integrated circuits eventually leading to component failure. A void growth model developed by engineers at Sandia National Laboratories is used to investigate the reliability of the aluminum conductor lines. Several computational methods for probabilistic analysis are investigated and the resulting reliability estimates of the interconnects are compared. The uncertainties in several critical design and manufacturing variables are modeled through statistical distributions and incorporated into the void growth model using first and second-order probabilistic methods. The results of this effort are then used to characterize the reliability of a conductor line in the presence of multiple void nucleation sites.

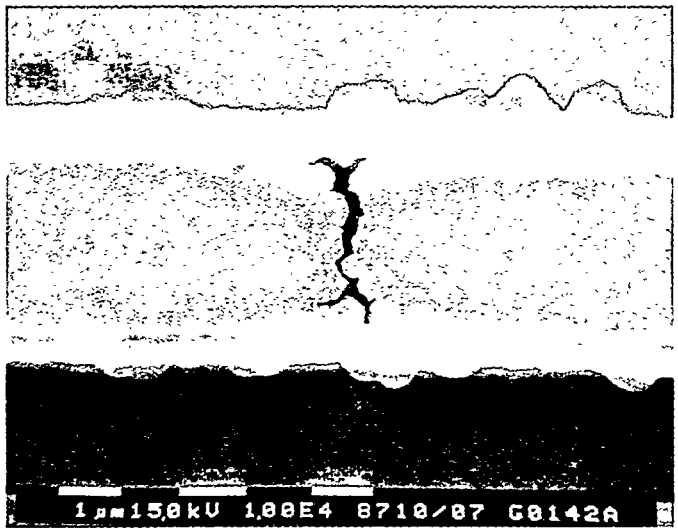

Figure 2.1 Typical crack-type interconnect void

Note: Since this initial effort was undertaken, the underlying model describing the growth of voids as a function of time has continued to evolve. However, the intent of this section is to demonstrate the potential for probabilistic analysis methods; these methods are independent of the true underlying void growth model. As new deterministic growth models are being developed, the approach used to characterize the reliability remains the same and continues to provide insight into critical manufacturing and material characteristics.

2.2 Background

Increasing miniaturization of silicon integrated circuits in recent years has led to the observation of void initiation and growth in aluminum conductor lines of these circuits. The voids assume two morphologies, either as a wedge-like form or a crack-like form, and grow as a result of thermal stress-driven mass diffusion. The aluminum conductor lines are typically passivated with a glass layer. The thermal expansion coefficient of glass is an order of magnitude smaller than that of aluminum. When the composite is cooled from the passivation deposition temperature (~700°K) to room temperature, a significant tensile stress is imparted on the aluminum. This stress field is not uniform and the stress gradient causes diffusive mass transportation. Also, the conductor lines are mechanically constrained by the glass layer, which prevents grain boundary sliding. These two features lead to void formation and growth in the aluminum conduction lines and affect their performance in electronic circuits. A typical interconnect void is shown in Figure 2.1.

The growth of voids in the aluminum interconnects is a time dependent phenomenon. Several types of variables influence the performance of the conductor lines: grain size, conductor length, initial stress, void shape, stress concentration, elastic modulus, operating temperature etc. All of these variables have uncertainties associated with them. The possibility of multiple void sites also needs to be considered. Therefore, the performance assessment of the aluminum conductor lines in the context of stress voiding can only be done in a probabilistic sense, i.e., through the estimation of reliability (or conversely the failure probability), given the statistical description of the underlying random variables.

2.3 Nucleation Process

2.3.1 Deterministic Description

A number of possible mechanisms have been proposed for the initiation of voids in a conductor line. Clearly one source of void growth that does not depend on nucleation involves the presence of grain boundary segregation of alloy constituents, impurities or incoherent precipitates. Alternatively, it is possible for voids to nucleate as a result of mass diffusion caused by excessive tensile stress. In a typical diffusion creep process the diffusion is balanced by grain boundary sliding. However, in the case of the conductor line this sliding is constrained by the passivation layer and the potential for a void nucleation exists.

2.3.2 Statistical Model

It is assumed that there is a finite number, N, of possible initiation sites in a conductor line of length y_l. The time until each possible initiation site nucleates, t_i, is a random variable with cumulative density function, $F_i(t)$. The probability that exactly k initiation sites will nucleate before time t can be characterized by a binomial distribution function:

$$\Pr\{(\text{number of nucleations before time t}) = \text{k}\} = \binom{N}{k}\left[F_i(t)\right]^k\left[1-F_i(t)\right]^{N-k} \quad [2.1]$$

The total area of the conductor line is assumed to be $2b \cdot y_l$. The grains are assumed to be circular with mean diameter, b. Then N is estimated as half of the total line area divided by the area of an individual grain.

A more realistic assumption would have been to assume that the number of possible initiation sites is a random variable correlated with line length and geometry of the conductor line as well as the grain size. However, there is insufficient data at this time to support the construction of such a statistical characterization.

2.4 Void Growth Kinetics

2.4.1 Deterministic Description

Once a nucleation site has been initiated, tensile stresses, induced by the disparate coefficients of thermal expansion of the passivation layer and the conductor line, contribute to void formation and growth. Yost et al. [1989a,b,c] constructed a stress-void kinetics model which leads to a closed form void growth expression. It is important to be aware that this model assumes that

these stresses are not significantly relaxed as voids propagate. There has been some recent experimental evidence that contradicts this assumption and the investigation into this is continuing.

The stress state in a conductor line is exacerbated by geometric features such as steps, contacts or corners. Using the presence of such a situation as a worst case scenario, the model for void volume $a^2(t)$ as a function of time proposed by Yost [1989c] is given in Equation 2.2.

$$a^2(t) = a_\infty^2\left[1+\left(\frac{\beta}{\lambda}\right)\left(1-\exp(-\lambda)\right)-\frac{2}{\pi}\sum_{m=0}^{\infty}\frac{C_m}{(2m+1)}\exp\left\{-tD(m+0.5)^2\left(\frac{\pi}{y_i}\right)^2\right\}\right] \qquad [2.2]$$

with:

$$C_m = \frac{4}{\pi(2m+1)}+\frac{\beta\left[(2m+1)\pi+(-1)^{m+1}2\lambda\exp(-\lambda)\right]}{\left[(m+0.5)^2\pi^2+\lambda^2\right]}$$

$$a_\infty^2 = \frac{2b\pi y_i\sigma_0(1-\nu)}{hE}$$

$$D = \frac{2EB}{\pi L(1-\nu)}$$

and the various parameters are defined:

$E = 75710\ MPa$

$\nu = 0.33$

y_i = line length = $500\mu m$

β = stress concentration factor = 1.0

$\lambda = y_i / b$

B = grain boundary diffusion coefficient = $6.19\times10^{-11}(\mu m)^3 / (MPa\cdot s)$

2.4.2 Statistical Model

Recent investigations [Korhonen. 1993] into conductor line voiding have assumed that the growth of voids is a deterministic process and can be characterized via a physics-based expression. However, this research assumes that both void nucleation and growth are random processes. Yost also performed a Monte Carlo analysis based on the void growth model presented here (Yost and Campbell 1990). However, no consideration was given to the relationship between the nucleation process and the subsequent void growth.

The probability of failure due to growth of a single void is defined as: $p_f = \Pr\left\{a^2(t) > a_{crit}\right\}$. Preliminary analysis highlighted three random variables as having the most dramatic impact on conductor line reliability. These variables are: grain size (L), initiation time (t_i), initial stress (σ_0), and a shape factor (h). The associated distributions and parameters are shown in Table 2.1.

Variable	Mean	COV	Distribution
Grain size-L (μm)	1.5	0.1	Lognormal
Initial stress σ_0 (MPa)	300	0.1	Lognormal
Shape factor h	1.2	0.1	Lognormal
Initiation time t_i (yrs)	10.0	1.0	Lognormal

Table 2.1 Definition of Random Variables

2.5 Multi-site Nucleation

Figure 2.2 depicts a typical situation that might exist in the case of multiple nucleation sites. As noted previously, prior investigations [Korhonen 1993] have assumed that conductor line failure resulted from the growth of a void from the first nucleation site. Under the assumption of stochastic void growth characteristics, this is clearly the exception rather than the rule.

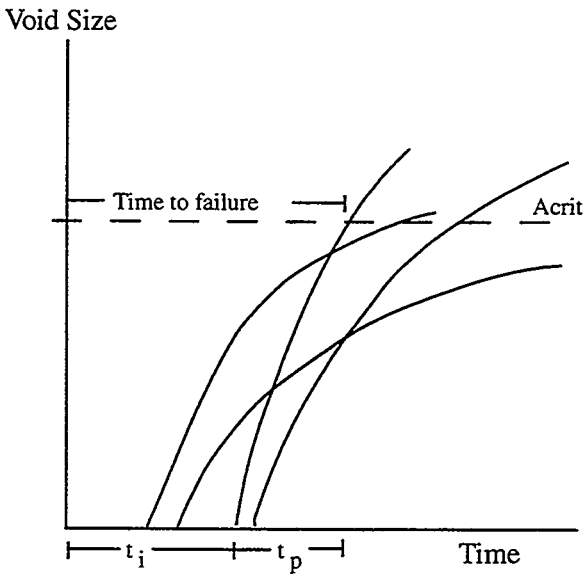

Figure 2.2 Failure Definition For Multi-site Damage

The reliability at time t of a conductor line of length y_i, is the probability that the minimum time for void nucleation and growth to a critical size of all k voids is greater than t:

$$R(t) = \Pr\{\text{no failures} \cup \min(t_0 + t_p) > t\} = \sum_{k=0}^{N} [1 - F_{t_0+t_p}(t)]^k \binom{N}{k} [F_{t_0}(t)]^k [1 - F_{t_0}(t)]^{N-k} \qquad [2.3]$$

where: $F_{t_0+t_p}(t)$ is the joint cumulative density function of $t_i + t_p$. (Note: Care must be when evaluating this expression for the case of no failures.)

2.6 Analysis

2.6.1 Approach

Statistically characterizing the life of aluminum conductor lines was accomplished in three stages:

1. Construction of a single void of the cumulative distribution function of void propagation time t_p. For different values of t, we compute the probability of the void size $a(t)$ being greater than or equal to a critical value a_{crit}, i.e. $P(a > a_{crit})$. This is in fact equal to $P(t_p < t)$, which is the CDF of t_p.

2. Computation of the cumulative distribution function of the total time for a void to reach a critical size, $t = t_i + t_p$, again for a single void. (The distribution of t_i describing the time to void initiation is assumed known)
3. Finally, computation of the interconnection reliability $R(t)$ using the multi-site model

2.6.2 General Analytical Techniques

Both first and second-order reliability methods [Robinson, 1998] were utilized to estimate the probability of failure (and subsequently the reliability) of a conductor line segment. The first-order method can be best described as a modification to the Rackwitz-Fiessler algorithm [Rackwitz and Fiessler, 1978]. Fundamental to the approach is the concept of a limit state function. Assuming the existence of a critical level of system performance, the limit state function partitions the system parameter domain $\mathbf{x} = (x_1, x_2, \ldots, x_n)$ into two regions: a region Ω where combinations of system parameters lead to an unacceptable or unsafe system response and a safe region $\overline{\Omega}$ where system response is acceptable. The probability of system failure is then defined by the expression:

$$p_f = \iint \cdots \int_{\Omega} f_{\mathbf{X}}(\mathbf{x}) d\mathbf{x} \qquad [2.4]$$

Perhaps the simplest way of explaining this approach is to examine the basic case of two independent random variables. Let R represent a random variable describing the strength of a system and let S represent a random variable describing the stress or load placed on the system. System failure occurs when the stress on the system exceeds the strength of the system: $\Omega = \{(r,s) \mid S > R\}$. Figure 2.3 depicts the concepts of a limit state function and the associated failure/success regions.

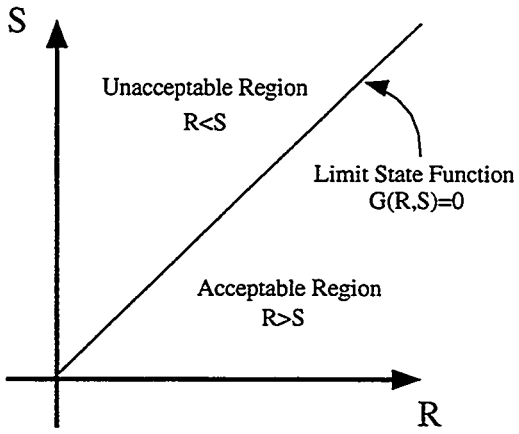

Figure 2.3 Limit State Function

The probability of failure is given alternatively by:

$$\begin{aligned} p_f &= \Pr\{R < S\} \\ &= \Pr\{R - S < 0\} \\ &= \Pr\{R/S < 1\} \end{aligned} \qquad [2.5]$$

where each of the algebraic expressions should give identical results. The limit state function is defined as that locus of points where:

$$G(R,S): R - S = 0 \qquad [2.6]$$

The first step is to transform the random variables to a set of independent random variables through an orthogonal transformation. These random variables are then normalized into a set of

reduced variables through the transformation: $u_i = \frac{x_i - \mu_i}{\sigma_i}$, where μ_i and σ_i are respectively the mean and standard deviation of the random variable, X_i. A new limit state function is then defined in terms of the reduced variables. In the above example, the limit state function becomes the locus of points where:

$$G(\mu_R + u_r\sigma_R, \mu_S + u_s\sigma_S) = G(r,s) = (\mu_R - u_r\sigma_R) - (\mu_S - u_s\sigma_S) = 0 \qquad [2.7]$$

and: $u_r = \frac{R - \mu_R}{\sigma_R}$ and $u_s = \frac{S - \mu_S}{\sigma_S}$. Since this is a linear transformation, no information has been lost. Graphically, the new limit state function appears in Figure 2.4. In the new space of basic variables, let the minimum distance from the origin to the limit state function be $|\beta|$. The point on the limit state that lies closest to the origin, $\mathbf{u}^* = (u_1^*, u_2^*, \ldots, u_n^*)$, is often referred to as the *most probable point* (MPP).

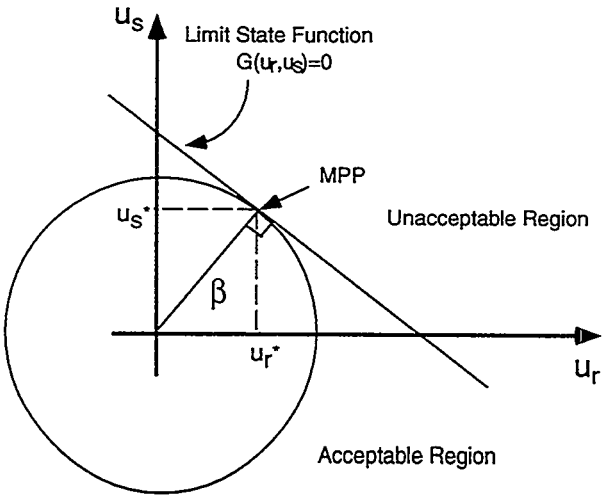

Figure 2.4 Safety Index

There is a direct relationship between the safety index and the probability of failure. As depicted in Figure 2.5, as β increases the limit state moves away from the origin and the probability of failure decreases. In general, this relationship is only approximate, but in the unique case of a linear limit state function and Gaussian distributed random variables, the relationship is exact: $p_f = \Phi(-\beta)$. In any case, this situation provides a convenient foundation for developing preliminary skills in analytical uncertainty methods. In addition, many preliminary analyses can be accomplished using these assumptions.

Returning to the simple example with two independent random variables, it is a simple problem in analytical geometry to show that the minimum distance from the origin to the limit state surface in reduced space is:

$$d = \frac{\mu_R - \mu_S}{\sqrt{\sigma_R^2 + \sigma_S^2}} = \frac{\mu_G}{\sigma_G} = \beta \qquad [2.8]$$

As previously mentioned, given a linear limit state and independent Gaussian distributed random variables, the probability of failure is given by:

$$p_f = \int_{\beta}^{\infty} \frac{1}{\sqrt{2\pi}} \exp\left(-\frac{w^2}{2}\right) dw = \Phi(-\beta) \qquad [2.9]$$

In general, the distance from the point $\mathbf{u}^*$ to the limit state $G(\mathbf{x}) = 0$ is given by the expression: $d = \sqrt{\sum_{i=1}^{n} u_i^*}$ (see Figure 2.6).

The difficulty then lies in determining the minimum distance for a general nonlinear function. This is essentially a nonlinear, constrained optimization problem:

$$\begin{aligned} &\text{minimize:} \quad d = \sqrt{\sum_{i=1}^{n} u_i^*} = (\mathbf{u}^{*T}\mathbf{u}^*)^{1/2} \\ &\text{subject to:} \quad G(\mathbf{u}) = 0 \quad \text{(equivalently } G(\mathbf{x}) = 0\text{)} \end{aligned} \qquad [2.11]$$

Shinozuka [1983] demonstrated that, in general, the minimum distance is given by:

$$\beta = \frac{-\nabla^{*T}\mathbf{u}^*}{(\nabla^{*T}\nabla)^{1/2}} = \frac{-\sum_{i=1}^{n} u_i^* \left(\frac{\partial G}{\partial u_i}\right)\Big|_{u=u^*}}{\sqrt{\sum_{i=1}^{n}\left(\frac{\partial G}{\partial u_i}\right)^2\Big|_{u=u^*}}} \qquad [2.12]$$

where the gradient is defined:

$$\nabla^{*T} = \left(\frac{\partial G}{\partial u_1}, \frac{\partial G}{\partial u_2}, \ldots, \frac{\partial G}{\partial u_n}\right)\Big|_{u=u^*}$$

Practically, the reliability index can be obtained with a Newton-type iteration algorithm known in reliability literature as the Rackwitz-Fiessler algorithm [Robinson, 1998].

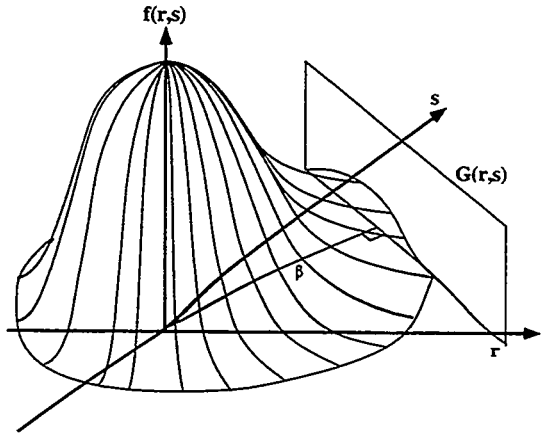

Figure 2.5 Depiction of joint probability density function and limit state function

First-order reliability methods perform well when the limit state surface has only one minimal distance point and it is nearly flat in the vicinity of the MPP. When the performance function is non-linear and/or when some of the x_i's are non-normal, a second-order approximation to p_f is obtained by approximating the limit-state surface with a second-order surface at MPP $\mathbf{y}^*$.

The second-order method was based on approximating the void growth equation with a second-order approximation and applying Breitungs' formula:

$$p_f = \Phi(-\beta)\prod_{i=1}^{n}(1-\beta\kappa_i)^{-1/2} \qquad [2.13]$$

where κ_j are the principal curvatures at the most probable point [Breitung, 1984].

Several other analytical and simulation-based methods have been developed for

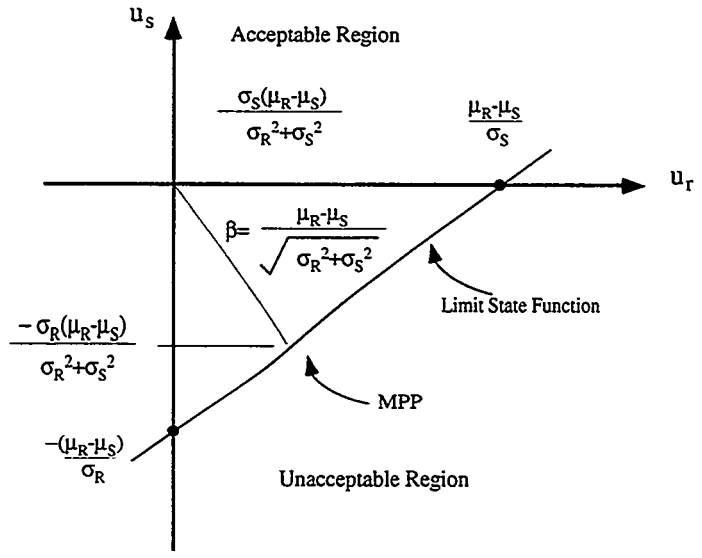

Figure 2.6 New Limit State Function

accurate estimation of the probability integral in Eq. 3.4, such as Advanced Mean Value method, Advanced First Order Reliability Methods (FORM), importance sampling, directional simulation, response surface approach etc. The above discussion has emphasized first-order and second-order methods (SORM) and captures the essential concepts of reliability computation. These techniques are widely used in structural and mechanical engineering applications. In this preliminary research, FORM and SORM are used for the stress voiding reliability analysis. The results of these methods are compared with those of basic Monte Carlo simulation.

2.7 Numerical Results

The computation of stress voiding reliability is performed along the three steps summarized in Section 2.6.

Step 1: For different values of t, we compute the probability of the void size $a(t)$ being greater or equal to a critical value a_{crit}, i.e. $P(a > a_{crit})$. This is in fact equal to $P(t_p < t)$, which gives the CDF of t_p. In this analysis, $a_{crit} = 1.0$ μm.

Based on the CDF of t_p, an 8th order polynomial curve-fit is computed for this CDF and differentiated to obtain the PDF. Using a Gaussian distribution approximation, the mean value and standard deviation of t_p can also be obtained. The mean value is taken as the value at cumulative probability 0.50, and the standard deviation is taken as the value of $t_{.84}$-$t_{.50}$. The mean and standard deviation value of void propagation time t_p are listed in Table 3.2.

Method	Mean	Std. Deviation
FORM	74.4	25.7
SORM	74.4	25.6
Monte Carlo	74.5	25.7

Table 2.2 Mean Value and Standard Deviation of Void Propagation Time t_p

Step 2: The CDF of total time t is also obtained by computing the probability of the response quantity being less than or equal to a given Value Z_0, $P(Z < Z_0)$. In this analysis, Z_0 is equal to 30, 40, ...90 years. The CDF plots of total time (initiation time + propagation time) using the FORM, SORM and Monte Carlo simulation methods are shown in the Fig. 2.7.

Step 3: Using the Eq. 2.3, the conductor line reliability is evaluated from 30 years to 100 years, and the plots of $R(t)$ with FORM, SORM and basic Monte Carlo simulation methods are shown in Fig 2.8.

2.8 Summary

This portion of the research emphasized the use of analytically-based probabilistic methods for assessing the stress voiding reliability of aluminum conductor lines in electronic circuits. First-order and second-order methods were described, and Yost's model for stress-voiding was assumed. The application of probabilistic computational methods to the stress voiding problem involved three steps, and the results of FORM and SORM methods were compared with Monte Carlo simulation results. The results indicate that analytical methods for probability computation have adequate accuracy and are an inexpensive approach to reliability estimation. Such an approach is especially valuable when the computational burden to compute the performance function become excessive.

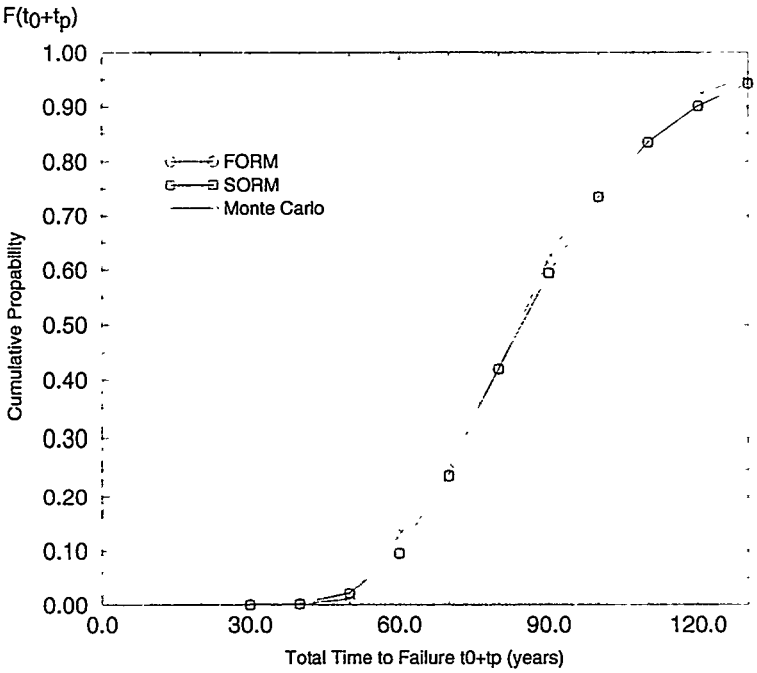

Figure 2.7 CDF for Single Void

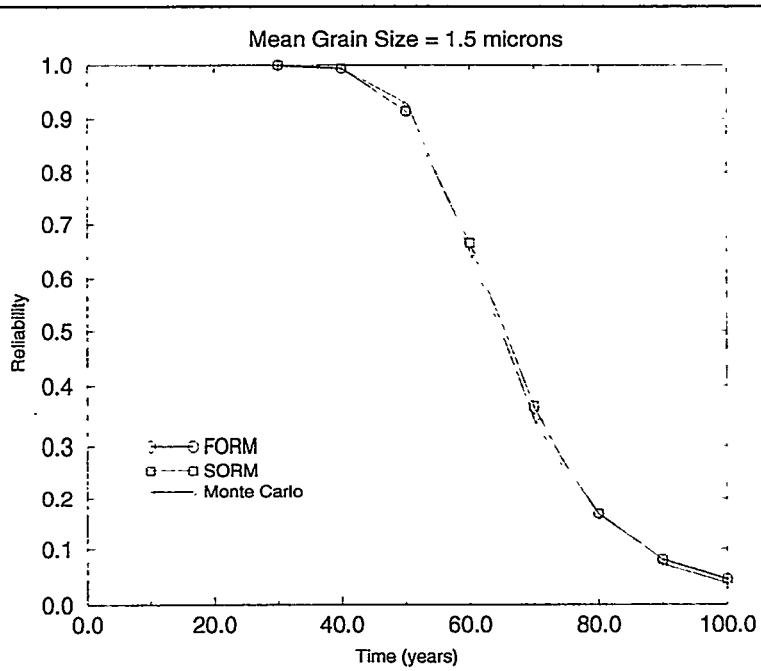

Figure 2.8 Estimation Total Reliability

3.0 Accelerated Aging of Polymers

3.1 Background

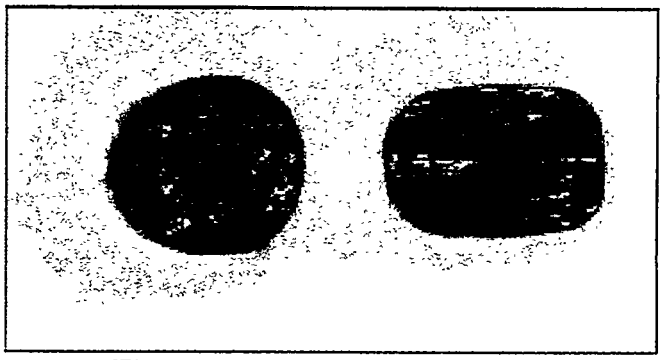

Figure 3.1 EPDM Cross Section Before/After Aging Set

Ethylene-propylene (EP) elastomers come in two basic types: ethylene-propylene copolymer (EPM) and ethylene-propylene terpolymer (EPDM). Both types are made up of a saturated chain of polymethylenes but the terpolymer also has a diene in the polymer side chain. These elastomers are random, amorphous polymers with outstanding resistance to ozone, aging and weathering. They also have good low-temperature flexibility and heat resistance and have excellent electrical properties. EP elastomers are common in a wide variety of applications including automotive parts, single-ply roofing, thermoplastic olefins and viscosity index improvers for lubricating oils. Of concern here is the application EPDM in o-ring seals.

Compression stress relaxation measurements provide perhaps the most representative characterization of the ability of the EPDM o-ring to maintain the required atmospheric integrity. However, while realistic, there are many complex interacting system elements (e.g. geometry or chemical and mechanical stresses) which preclude characterizing the life of this system at ambient temperature and loading environments. Alternative testing and analysis approaches are necessary to gain a quantitative understanding of the mechanism associated with system aging and performance degradation.

In addition, the actual environment and stress conditions under which the o-rings will be required to operate can not be completely described. The uncertainty in operating conditions coupled with limited understanding of the complex physical and chemical processes associated with o-ring aging supports the use of probabilistic-based methods for characterizing the life of o-rings in a storage environment. As always, the goal is to anticipate when problems may occur as an alternative to delaying action until the problem becomes a critical reliability issue.

For this effort, failure is assumed to occur when the sealing force between the o-ring and metal mating surface drops below a critical level. For practical purposes, the parameter of interest will be the normalized restoring force $f(a,T) = F(a,T)/F_0$ as a function of age a and temperature T. Unless specifically noted, all temperatures are in degrees Kelvin. It will be assumed that, for a particular system age, $f(a,T)$ is a random variable with probability density function: $g(f,a;x,n)$ where the distribution parameters, x, n are implicitly assumed to be functions of age, a, and temperature, T.

3.2 Degradation Function Analysis

Preliminary deterministic investigations into the aging process associated with EPDM o-rings suggested that, for this material, aging is composed of two performance regimes. This might

occur as a result of two underlying chemical processes, one which dominates early in the life, while the other chemical process dominates during the later stages of o-ring degradation. The age at which the transition occurs might also be expected to be a characteristic unique to a specific material. A mixture of functions describing o-ring performance was therefore investigated. In particular, the following general functional form was assumed:

$$f(a,T) = W_1 \exp\left[-\left(\frac{a}{d_1(T)}\right)^{\beta_1}\right] + W_2 \exp\left[-\left(\frac{a}{d_2(T)}\right)^{\beta_2}\right] \qquad [3.1]$$

where: $W_1, W_2 \left(\sum W_i = 1\right)$ are weights reflecting the relative impact of each aging regime. The exponent parameters, β_i, roughly reflect the rate at which aging occurs during a particular segment of the o-ring life. The larger the value of β_i the slower the rate of degradation. The parameters $d_i(T)$ are functions of the temperature at which the system operates and serve to shift the function $f(a,T)$ up or down the time scale as required for a particular testing/operating temperature.

The first step in the analysis involves estimating the parameters of the general aging expression represented by Equation 3.1. Accelerated testing was performed at two temperatures: 111C° and 125C°. Data were available describing the normalized restoring force as a function of o-ring age. A nonlinear least squares analysis was used to simultaneously fit the equations to both sets of data. The results are depicted in Figure 3.2 and the parameter estimates are summarized in Table 3.1. In addition to these parameters, the weights were estimated to be: $W_1 = W_2 = 0.5$.

Temperature (C°)	$d_1(T)$	$d_2(T)$	β_1	β_2
T=111	126	509	1.0	5.1
T=125	22	151	0.8	3.0

Table 3.1 Parameter Estimates

Critical to the analysis is the characterization of the acceleration parameters in Equation 3.1. The limited amount of data makes this particularly difficult. With the very sparse data, it is necessary to assume that the parameters characterizing the aging rates in the different regions are not functions of the operating temperature: $\beta_i(T) = \beta_i$. In particular, the aging rate parameters were approximated by the average values over 111 and 125°C:

$$\beta_1 = \frac{\beta_1(111) + \beta_1(125)}{2} = 0.90$$
$$\beta_2 = \frac{\beta_2(111) + \beta_2(125)}{2} = 4.05 \qquad [3.2]$$

Application of these values in the regression equations for the test data did not result in a significant error in the functions used to characterize the experimental data.

An extensive review of a variety of potential functions describing the location parameter $d_i(T)$ was undertaken. Again, the limited amount of experimental data suggested a very simple form: $T = a + b\ln(d)$ or:

$$d_i(T) = \exp\left\{\frac{T - a_i}{b_i}\right\} \qquad [3.3]$$

where: a_i, b_i are parameters to be estimated. Figure 3.3 presents a graphical view of the data and the final functional estimates. Given estimates of the acceleration rate parameters and the shift parameters as a function of temperature, T (Kelvin), a functional characterization of the

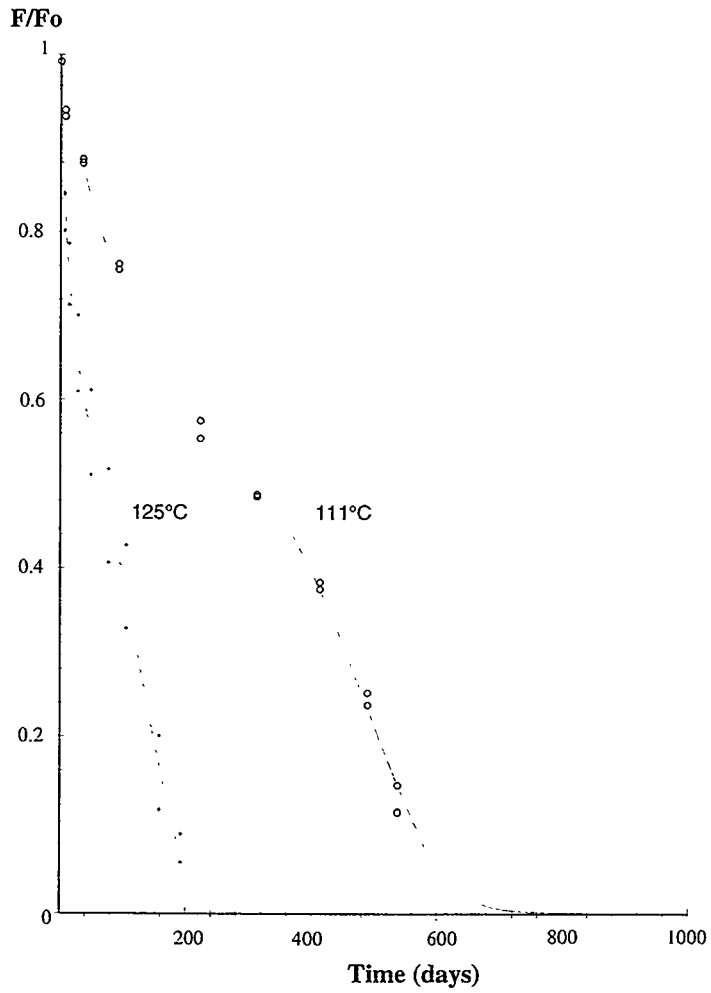

Figure 3.2 Initial Aging Analysis Results

mean aging function is available:

$$f(a,T) = W_1 \exp\left[-\left(\frac{a}{d_1(T)}\right)^{\beta_1}\right] + W_2 \exp\left[-\left(\frac{a}{d_2(T)}\right)^{\beta_2}\right]$$
$$= 0.5\left\{\exp\left[-\left(\frac{a}{d_1(T)}\right)^{0.9}\right] + \exp\left[-\left(\frac{a}{d_2(T)}\right)^{4.05}\right]\right\} \quad [3.4]$$

where:

$$d_1(T) = \exp\left[\frac{436.82 - T}{11.52}\right]$$
$$d_2(T) = \exp\left[\frac{455.95 - T}{11.52}\right] \quad [3.5]$$

With this information, a deterministic characterization of the average degradation of the EPDM o-rings can be accomplished. Figure 3.4 summarizes the results for temperatures of 25, 37 and 50°C.

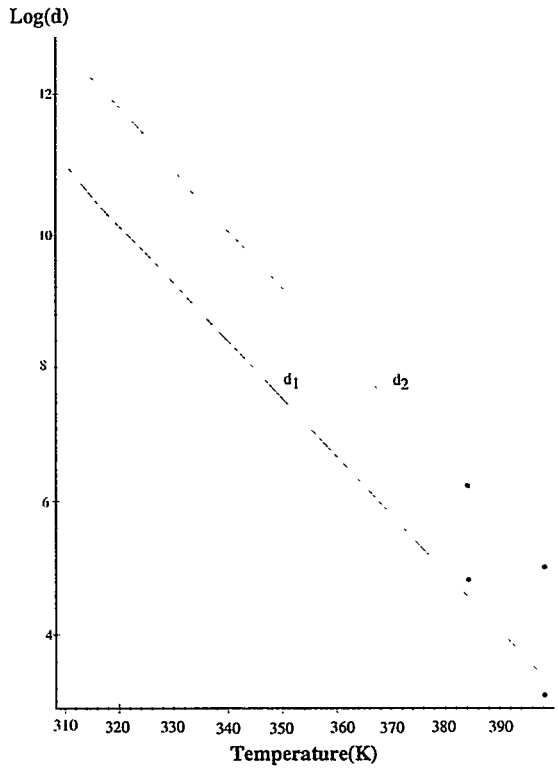

Figure 3.3 Shift Parameter Function Estimation

3.3 Uncertainty Function Analysis

It will be assumed that the mean of the distribution as a function of temperature and system age is given by Equation 3.4. The difficulty then is to characterize the confidence in the predicted restoring force based on the limited data available at 111 and 125°C. As noted earlier, it will be assumed that, for a particular system age, $f(a,T)$ is a random variable with probability density function: $g(f,a;x,n)$ where the distribution parameters, x, n, are implicitly assumed to be functions of a and temperature, T. The underlying distribution is assumed to be:

$$g(f,a;x,n) = \frac{\Gamma(n)}{\Gamma(x)\Gamma(n-x)} f^{x-1}(1-f)^{n-x-1} \quad [3.6]$$

where: $0 \le f \le 1$, $n > x > 0$. This is the beta distribution with mean and variance, $\mu_f = \frac{x}{n}$ and $\sigma^2 = \frac{x(n-x)}{n^2(n+1)}$ respectively. For convenience it is noted that the parameters of the distribution in terms of the first and second moments are given by the expressions: $x = \frac{\sigma^2\mu^2 + \mu - 1}{\sigma^2\mu^3}$ and $x = \mu n$.

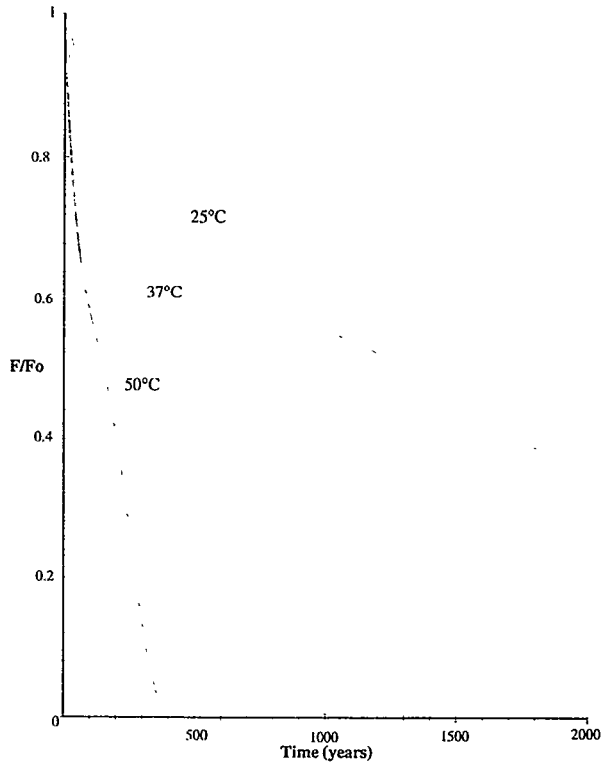

Figure 3.4 Sample Aging Analysis Results

Given the limited amount of data, it is difficult to justify a complex relationship between the acceleration temperature and both the distribution mean and variance. The relationship between acceleration temperature and distribution mean is consistent with the limited data and can be reasonably explained with the underlying chemistry. However, there is not sufficient data to gleam a significant relationship between distribution variance and acceleration temperature.

Test data for the restoring force was grouped into 10 equally spaced intervals. For each interval, the mean and variance of the data was estimated. When test regimes with similar means are compared, as summarized in Table 2, there does not appear to be a significant change in the variance of the underlying density function as the acceleration temperature changes.

The expected time for the material to reach the mean restoring force for a given operating temperature can be obtained from Equation 3.1. In addition, given the mean restoring force, the associated variance can also be estimated. As new data becomes available, these variances can be updated to reflect the increased confidence in the estimates of system aging.

Temperature	Mean	Variance
125	0.7499	0.0625
111	0.7591	0.0609
125	0.5608	0.0821
111	0.5647	0.0819
125	0.3777	0.07835
111	0.3792	0.07847

Table 3.2. Comparison of Temperature, Mean and Variance

3.4 Results and Discussion

The characterization of the mean restoring force as a function of temperature and age can then be coupled with the description of the variance of the restoring force. The final results are presented in Figure 3.6 for an operating temperature of 25°C. In addition, since failure is defined as a normalized restoring force less than 0.1, the probability of observing a failure is also presented as a function of system age. These results are also summarized in Table 3.3. Note that the probability bounds expand in the region of $F/F_0 \approx 0.6$ due to the limited test data in this interval.

Age (yrs)	8.99	50.6	112.8	252.4	383.1	546.7	668.5	814.7	938.6	1009.1
$P(F/F_0 < 0.1)$	9x10^-6	0.00016	0.0003	0.49	0.16	0.048	0.15	0.36	0.65	0.79

Table 3.3 Probability of Failure versus System Age

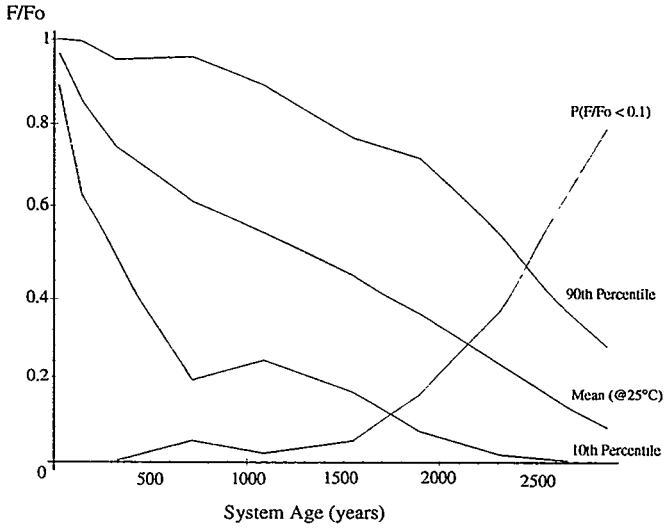

Figure 3.6 Summary of Results for 25C

It is critical to remember that these results are based on a very limited amount of data. In particular, the following assumptions are critical to the analysis:

1. The mean life can be described by a mixture of exponential functions (Equation 3.4). This appears to be a reasonable assumption based both on the actual data and possible chemistry changes as the material ages
2. Only the parameters $d_i(T)$ vary with temperature and are described via simple exponential functions. With the limted data it is difficult to justify a more complex relationship. It is quite likely that the $\beta_i(T)$ are not constant as assumed, but are also functions of temperature.
3. The underlying density function is beta. The beta provides an extremely flexible density function encompassing a variety of common density functions (e.g. uniform). However, since the density function is bounded between 0 and 1, the resulting probability bounds can be misinterpreted for upper and lower values of F/F_0. As seen in Figure 3.6, the tight upper bounds for the extreme system age is an artifact of the lower 'zero' bound on the beta density function and, obviously, not an indication of the amount of data available.

3.5 Summary

The above analysis is unique from classical accelerated aging reliability analyses and has illustrated a number of points. First, the availability of (or lack of) experimental data can and should be reflected in the final reliability analysis. This is not possible in traditional Arrhenius analyses. As evident in Figure 3.6, the confidence bounds about the mean value clearly highlight where information is/is not available for decision making. Since, even considering the lower confidence bound, there was not cause for concern, additional testing was not required. (As noted earlier, the tight upper bounds for the extreme system age is an artifact of the lower 'zero' bound on the beta density function and do not reflect the amount of data available.) Second, statistical methods, when properly applied, can provide insight into subtle changes in the

underlying physical failure process. The appearance of the 'knee' in Figure 3.2, is contrary to the traditional aging analyses performed on most materials (not just polymers as in this effort). However, knowledgeable examination of the underlying chemistry by Sandia chemical engineers led to a likely explanation and particular questions were raised about how polymer performance degrades as a function of time.

4.0 Reliability Degradation Due to Atmospheric Corrosion

4.1 Introduction

Corrosion is defined as the deterioration of a substance or its properties due to a reaction with its environment. Atmospheric corrosion is one of the primary age-related degradation modes observed in the nuclear weapons stockpile. Corrosion-induced failure is becoming a critical issue because of the direct consequence to function and therefore reliability. The recent adoption of commercial off-the-shelf (COTS) hardware by the DOD will likely result in the need for the DOE to use plastic-encapsulated microelectronics (PEM) in future weapon systems and upgrades. The plastic formulations used in PEMs have a finite permeability to moisture. As such, the devices, with micron and sub-micron sized metallization features, have a related susceptibility to environmental degradation.

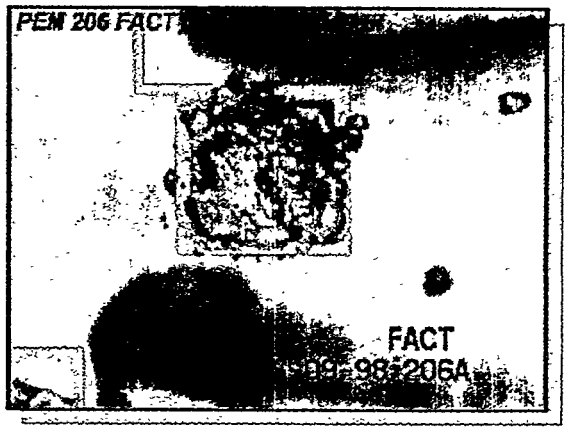

Figure 4.1 Corrosion of Bondpad

The focus of this section is on the description of a physics-based model that describes moisture-related metallization failure phenomena in PEM devices with a focus on corrosion of aluminum bondpads, and use of probabilistic methods to characterize the impact of these failure mechanisms on the storage reliability of PEM devices.

4.2 Background

Although one of the system design criteria is to ensure that all materials are compatible with the expected environment, corrosion typically still occurs because the local environment does not remain as expected (e.g., results from a bad seal, internal material outgassing). The traditional approach has been to assess the severity and potential consequences of corrosion problems that arise and then, if needed, change materials or the environment. The basis for the assessment is normally engineering judgment that utilizes historical evidence, failure analyses, accelerated aging, and sometimes limited empirical correlations. In the future our high standards for surety will require the development of sophisticated computer models for weapon reliability predictions which, in turn, will include accurate corrosion failure models and input data.

Although corrosion of structural and mechanical components occurs, it is the corrosion of electronic components that is currently the primary concern because of the direct consequence to function and therefore reliability. In general, the electronic features that are susceptible to corrosion degradation contain copper and silver (sulfidation) or aluminum (localized pitting). Of particular interest is corrosion-induced failure of microelectronic devices. In the past, Military Specification microelectronics were available in hermetically sealed ceramic packages. However, the adoption of the Perry Initiative by the DOD requires that COTS hardware be used when possible, including microelectronics that are encapsulated with plastic molding materials.

The widespread adoption of these PEM devices in uniquely military applications will soon eliminate the availability of the classical hermetically sealed packages. As such, COTS microelectronics will likely be incorporated into future DOE weapon systems and upgrades. The plastic formulations used in PEMs have a finite permeability to moisture and cracks are often present between the plastic and metal feed-through features. As such, the devices, with micron and sub-micron sized metallization features, have a related susceptibility to environmental degradation.

Long term storage in an unpowered state is the major concern with the use of PEM devices in nuclear weapons. The microelectronics industry has concentrated on the operational reliability and has not been overly concerned with the issues associated with the dormant storage of PEM devices.

A number of studies have been completed that suggest the operational reliability of PEM devices may not be an issue. These analyses have concentrated on accelerated aging techniques employed in conjunction with simple empirical statistical analyses. However, no real link to actual environmental conditions exists. PEM operational reliability approaches that for hermetic packaged devices in many environments and actually exceed hermetic devices in some special environments, such as high shock. However, because most consumer and industrial electronic devices are continuously or at least periodically electrically active, industrial motivation to assess long-term storage reliability has not existed and the extent and impact of corrosion during these periods is virtually unknown.

Stockpile storage is characterized by extended periods of electrical inactivity (lack of any sustained bias voltage) and the existence of a dynamic and changing chemical and thermal environment. For the case of corrosion, bias voltage is important because the intrinsic ohmic heating that occurs during operation usually dries the device, but also can cause enhanced electrolytic dissolution. Given these factors, the statistical information and type of empirical treatment associated with the operational phase are not applicable. In particular, the elimination of any ohmic heating raises serious concerns about the effect of corrosion (moisture-induced degradation of metallization) on the storage reliability of PEM devices used in military hardware. Historically during accelerated aging, two types of moisture-related phenomena have been observed: *Au* wire/*Al* bondpad interfacial degradation and distributed *Al* track corrosion. The track corrosion is believed to be related to moisture penetration through defects in the protective *SiN* passivation layer and the presence of contamination. Importantly, modern best commercial practice has effectively eliminated track corrosion as a significant failure mechanism. Bondpads have no passivation treatment and are susceptible to intermetallic voiding and accelerated attack due to moisture-related galvanic effects.

4.3 Analysis Approach

The following analysis represents a very simple approach to a very complex problem. As more data becomes available to support a more detailed failure physics analysis, additional reliability analyses will be conducted.

4.3.1 Generation of Defects

The number of defects in the plastic encapsulation is assumed to occur according to a Poisson probability density function:

$$\Pr\{N=k\}=\frac{e^{-\alpha x}(\alpha x)^k}{k!}, \qquad \alpha>0, k=0,...,\infty \qquad [4.1]$$

where α is the rate (defects/unit area) at which defects occur in the plastic encapsulation and x is the area of interest. The k defects are then evenly distributed (in the statistical sense) across the area of interest. A two-dimensional quasi-Monte Carlo scheme based on Hammersley sequence is used since it provides an optimum distribution of defects throughout x. If the projection of this area onto the op-amp results in the coincidence of one or more defects and a bondpad, corrosion is assumed to initiate at that pad.

However, for this first analysis, the area to be considered has been divided into an $n \times n$ discrete grid and the pad locations are given by specific elements in the grid. Therefore, since the number of defects must be finite and n is relatively small, the number of defects is assumed to be a random variable characterized with a binomial distribution:

$$\Pr\{N=k\} \approx \frac{N!}{k!(N-k)!} p^k (1-p)^{N-k} \qquad p \geq 0, k=0,\ldots,N \qquad [4.2]$$

where: $N = n \cdot n$ and $\alpha x \approx Np$. A random number of defects, k, are chosen and an N-dimensional vector of zeros is generated with the first k elements equal to 1. The vector is then 'shuffled' and reformed into an $n \times n$ matrix. The resulting matrix has elements indicating the location of a defect and if this corresponds to the location of a bondpad, corrosion is assumed to initiate at that pad.

4.3.2 Corrosion Growth

Given that corrosion at a bondpad has initiated, the rate of change of the pad resistance as a function of time is assumed to follow the following physical relationship:

$$\frac{d\Delta R}{dt} = k \cdot P_c \cdot \exp\left(-\frac{Ea}{R \cdot T(t)}\right)\left\{1-\exp\left[-\left(\frac{H(t)}{\eta}\right)^{\beta}\right]\right\} \qquad [4.3]$$

where the ambient temperature follows the relationship: $T(t) = T_m + T_a \sin(\omega_T t + T_0)$ and the relative humidity has the form: $H(t) = H_m + H_a \sin(\omega_H t + H_0)$. Since a solution to $\frac{d\Delta R}{dt}$ is difficult to find, a numerical integration is performed at each point in time.

4.3.3 Multi-site Damage

Failure of pad i occurs when the resistance of that pad drops below the unique critical level required to perform the function associated with pad i. The operational amplifier fails at that first instance when the resistance of any pad drops below the critical level: $t_f = \min\{t_1,\ldots,t_8\}$

However, the degradation of the resistance of a pad is a random function of environmental factors, corrosion physics and the presence of defects in the encapsulation. Therefore the time at which each pad reaches a critical resistance is a random variable and at each time there is a finite probability that the op-amp will fail. In addition, it is assumed that corrosion on each pad will lead to failure independent of the corrosion on other pads. The probability that the component fails before time t is then given by:

$$
\begin{aligned}
p_f &= \Pr\{t_f < t\} = \Pr\{\min\{t_1,\ldots,t_k\} < t \mid k \text{ bond pads with defects}\} \\
&= 1 - \Pr\{\min\{t_1,\ldots,t_k\} > t \mid k \text{ bond pads with defects}\} \\
&= 1 - \Pr\{(t_1 > t) \cap (t_2 > t) \cap \cdots \cap (t_k > t)\} \\
&= 1 - \Pr\{t_1 > t\}\Pr\{t_2 > t\}\cdots\Pr\{t_k > t\} \\
&= 1 - \prod_{i=1}^{k}[1 - F(t_i)]
\end{aligned}
\qquad [4.4]
$$

Note that this is a compound stochastic process. The probability of failure can be represented by a simple parallel system of k 'units'. However, k is random variable and is a function of the density of defects present in the plastic encapsulation. A closed form solution for this particular probability problem is not available and we must resort to simulation.

The first problem is to characterize the cumulative density function for the time to failure of an individual pad assuming that a defect occurs in the vicinity of the pad. By examining how this probability of failure changes as a function of time, it is possible to characterize the cumulative density function for a particular pad.

4.4 Solution

The external temperature and humidity $T(t), H(t)$ were simulated as first-order, autoregressive stochastic processes (correlated over time). Based on this underlying process, samples of temperature and humidity were simulated for each time period. Using these values, the differential equation describing the change in pad resistance as a function of time, Equation 4.3, was solved numerically. The result is a realization of the resistance of a pad after aging for a particular length of time. This process was repeated at daily intervals over the course of a number of test years.

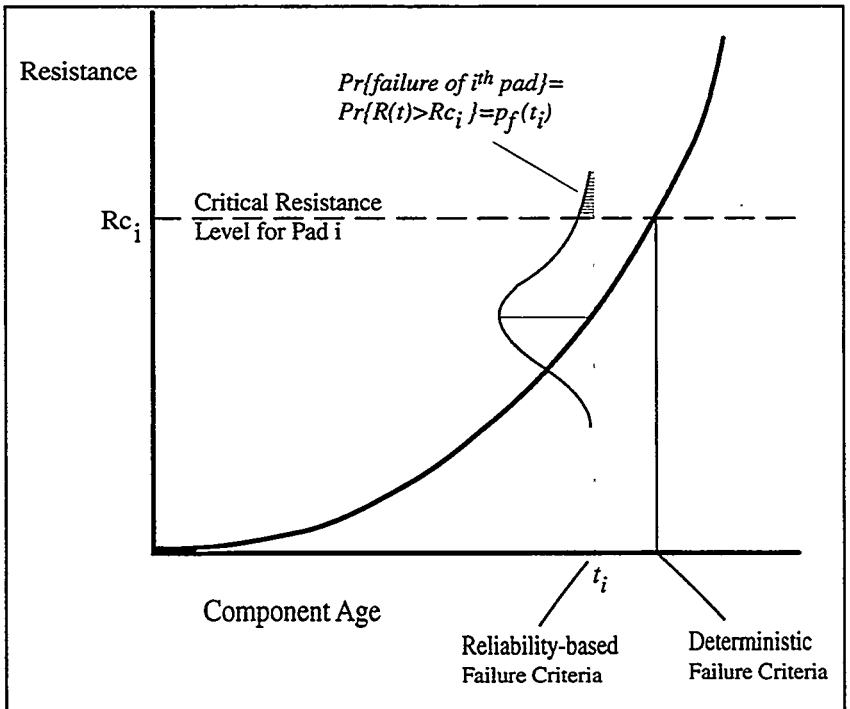

Figure 4.2 Generation of CDF for Single Bondpad

For a particular time the probability of failure for a single bondpad is depicted in Figure 4.2. When combined with the other bondpads via Equation 4.4 the resulting cumulative distribution function is depicted in Figure 4.3.

4.5 Summary

The aging degradation of the plastic encapsulated microcircuits can be characterized in a straightforward fashion using modern reliability and uncertainty analysis techniques. This effort was not a direct as the other approaches outlined in this document; the time correlated temperature and humidity random variables were an additional complication. An additional complication was the stochastic differential equation that characterized the changing pad resistance as a function of age. The repeated numerical solution was time consuming and greatly

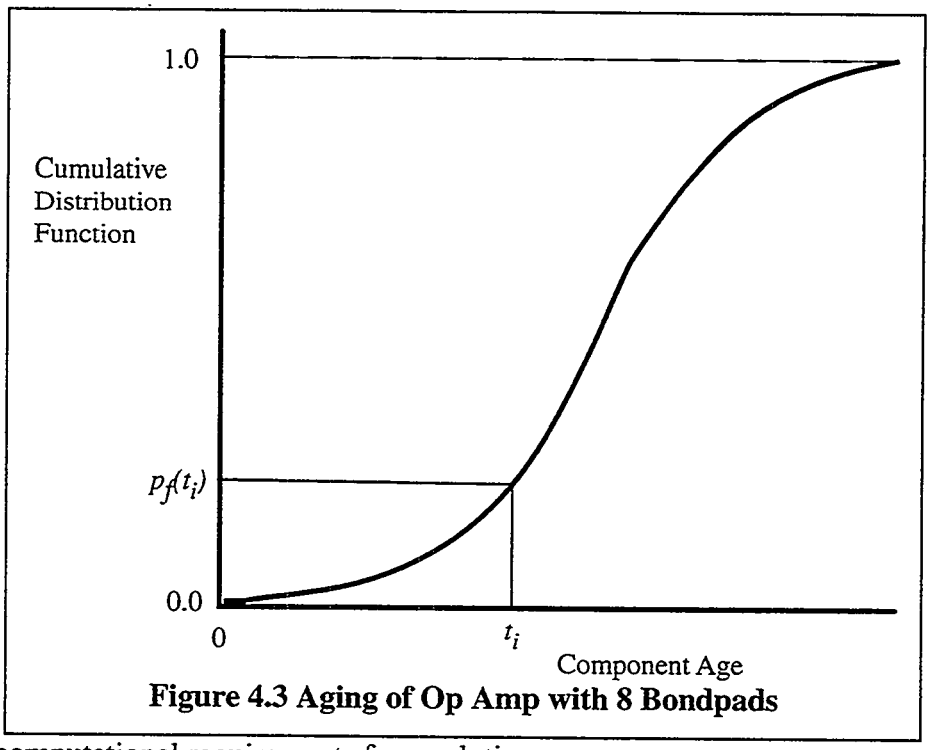

Figure 4.3 Aging of Op Amp with 8 Bondpads

added to the computational requirements for a solution.

However, both of these issues were easily addressed by incorporating the necessary analysis routines into a common software analysis routine being developed at Sandia. This software is the subject of the following final section of the report.

5.0 Cassandra Reliability Analysis Software

5.1 Introduction

As alluded to in the Chapter 1, Sandia National Laboratories has been moving toward an increased dependence on model- or physics-based analyses as a means to assess the impact of long-term storage on the nuclear weapons stockpile. These deterministic models have also been used to evaluate replacements for aging systems, often involving commercial off-the-shelf components (COTS). In addition, the models have been used to assess the performance of replacement components manufactured via unique, small-lot production runs. In either case, the limited amount of available test data dictates that the only logical course of action to characterize the reliability of these components is to specifically consider the uncertainties in material properties, operating environment, etc. within the physics-based (deterministic) model. This not only provides the ability to statistically characterize the expected performance of the component or system, but also provides direction regarding the benefits of additional testing on specific components within the system. An effort was therefore initiated to evaluate the capabilities of existing probabilistic methods and, if required, to develop new analysis methods to support the inclusion of uncertainty in the classical design tools used by analysts and design engineers at Sandia. The primary result of this effort is the CRAX (**C**assandra **Ex**oskeleton) reliability and uncertainty analysis software.

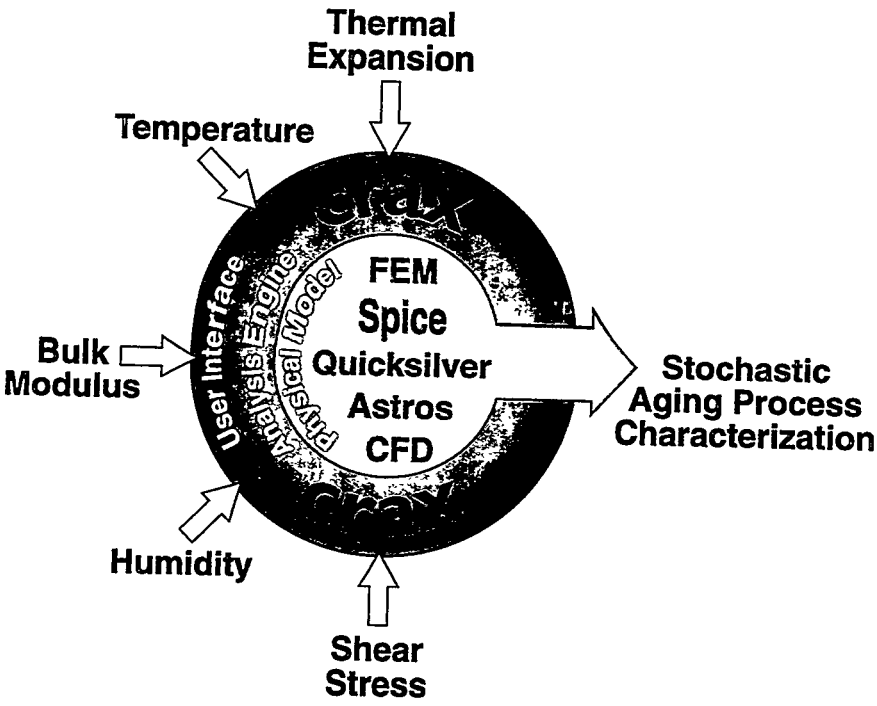

Figure 5.1 Relationship Between Software Elements

5.2 Background

Traditional reliability methods depend on the collection of a large number of samples or observations to characterize the existing condition of the weapons stockpile. These tests provide a snapshot of the existing reliability characteristics of the system. A major objective of recent research is to develop mathematical techniques and computer analysis tools to anticipate stockpile problems before they become critical issues [see Figure 1.1]. The assessment of new materials, manufacturing techniques have, in the past, depended on 'average' characterization using deterministic modeling tools. Recent research, however, has focused on developing mathematical methods for incorporating uncertainty in traditional deterministic modeling, in

particular, the advanced phenomenological modeling and simulation techniques used to characterize the physics of the underlying failure processes.

Of particular concern was the development of an analysis capability that would be applicable over the entire life-cycle of the system. An essential element was the ability to incorporate both test data and engineering judgement into the reliability characterization of the material or component being evaluated. Finally, it was important that the method address the sensitivity of the system performance to the uncertainties in the various internal and external model parameters.

As part of the Enhanced Surveillance Program, an effort was initiated to develop new software tools to support the inclusion of uncertainty in the classical design tools used by engineers at Sandia National Laboratories. The primary result of this effort was the CRAX/Cassandra analysis software.

5.3 Software Elements

There are three major elements to CRAX: 1) the uncertainty analysis engine – Cassandra, 2) the user interface – also called CRAX, and 3) the physical model. The relationship between these three elements is depicted in Figure 5.1.

The heart of the CRAX software is the Cassandra uncertainty analysis engine. This engine consists of a number of software routines that permit the user to select a variety of methods for including uncertainty in their analyses. A number of first and second order techniques, max-likelihood and a variety of other analytical methods are available for application. In addition, there are options for using a number of pseudo- and quasi-Monte Carlo methods. Specific methods are constantly being updated and improved. (One of the more recent additions is the option to use quasi-Monte Carlo sampling methods rather than traditional pseudo-Monte Carlo techniques [Robinson and Atcitty, 1999]) Cassandra is written completely in C/C++ making the engine very portable.

CRAX/Cassandra has been used with Win95, WinNT, Power Macintosh, Sun, Silicon Graphics and DEC operating systems. In addition, the software has been ported to one of the large tera-flop computers at Sandia.

Access to the Cassandra uncertainty analysis engine is gained via the CRAX interface. The CRAX graphical user interface (GUI) is based entirely on the Tool Command Language (Tcl) and associated Tool Kit (Tk). The use of Tcl and Tk permits the software to be hosted on any platform and provides a great deal of flexibility in accessing the Cassandra uncertainty engine. Rather than trying to develop a complicated GUI for the user that could handle any situation, the use of Tcl/Tk permits the very quick construction of unique interfaces specific to the problem being analyzed. (A basic/generic interface is available for simple analyses.)

The last element in the CRAX family is the physical model. It was decided early in the development of CRAX to not include any physical modeling tools directly in the software. Rather than develop a modeling tool (e.g. a finite element or thermal analysis package) unique to CRAX, it was decided to let the engineer rely on the existing tools that they were comfortable with and had confidence in. While not the ideal situation in terms of analysis speed, it was felt that for the engineers to become comfortable with incorporating uncertainty into their deterministic models, it was critical to not stretch their belief system too far. The CRAX GUI

effectively 'wraps Cassandra around' the existing analysis software; hence the reference to CRAX as an exoskeleton.

5.4 Cassandra Capabilities

The data for Cassandra is input via the graphical user interface, CRAX. Figure 5.2 depicts the input/output options available. Existing analyses can be loaded from a text file and subsequent analyses can be saved as an input file or in a variety of special formats for input to other analysis programs. The plots can be saved as a postscript file for later inclusion in reports. The CDF can be saved for later processing in a system level analysis program. In addition to color scheme information, the network locations (IP addresses) of the computers performing the uncertainty analysis and the performance analysis can be input interactively and changed 'on the fly'.

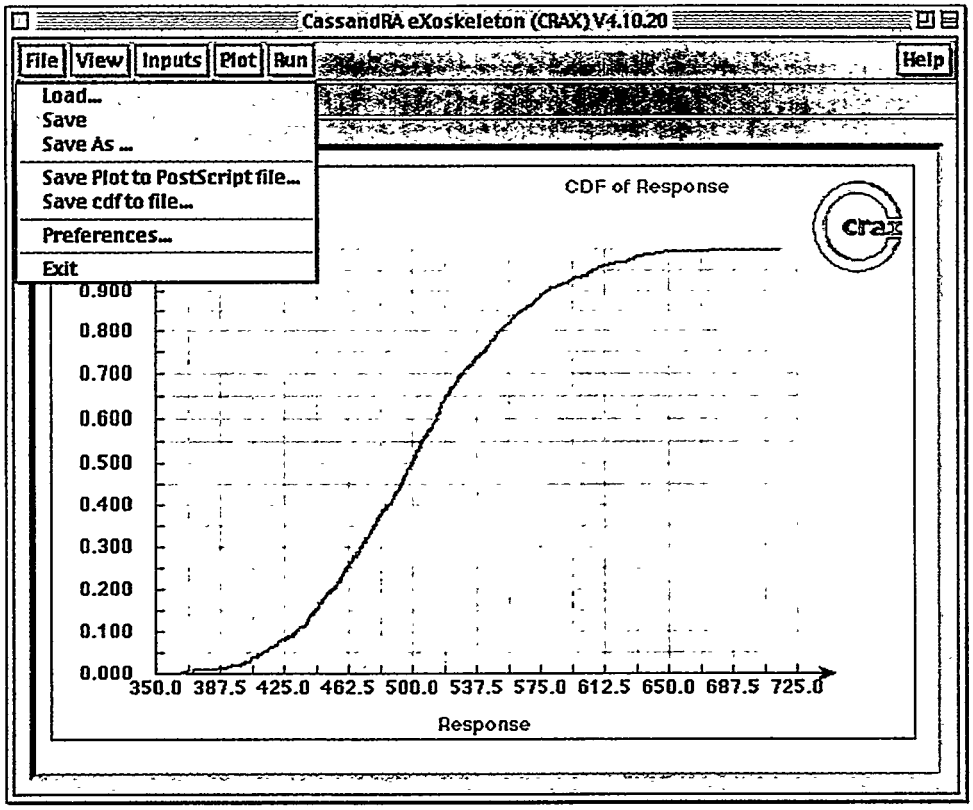

Figure 5.2 Input and Preference Options

The capability exists to view any of the input or output files that are generated during the course of the analysis using a built in file browser. Input options (see Figure 5.3) provide the user with a wide range of capabilities.

- The user can choose from a variety of particular analysis methods (e.g. analytical or Monte Carlo). These methods are constantly being updated and new methods are continuously being added (Figure 5.4).

- Characterizing the underlying random variables in terms of distribution and moments is easily accomplished with a specific interface menu and additional distribution types can be easily added as required (Figure 5.5).
- The user also has the capability to set the various deterministic parameters.
- Characterization of the correlation structure between random variables is done through an interactive window presentation of the correlation matrix.
- An option unique to the Generic CRAX model option is the ability to input the actual performance function to be analyzed. This is a simple alternative available for those situations where a complex computational algorithm subroutine is not required for system performance evaluation (Figure 5.6).

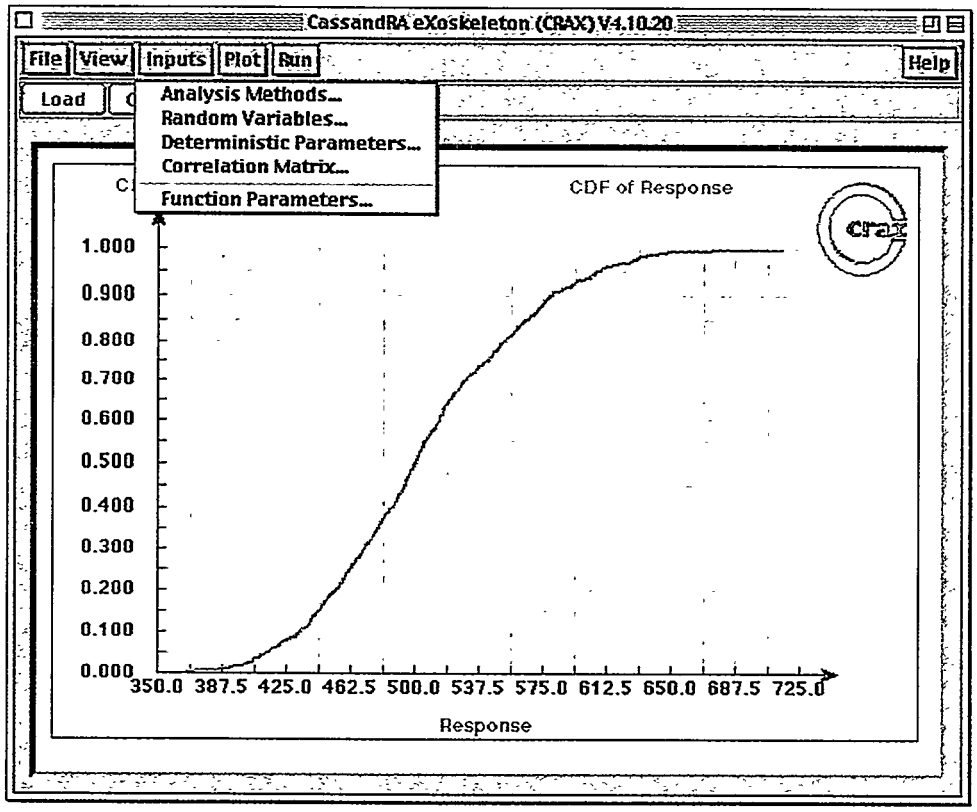

Figure 5.3 Input Data Options

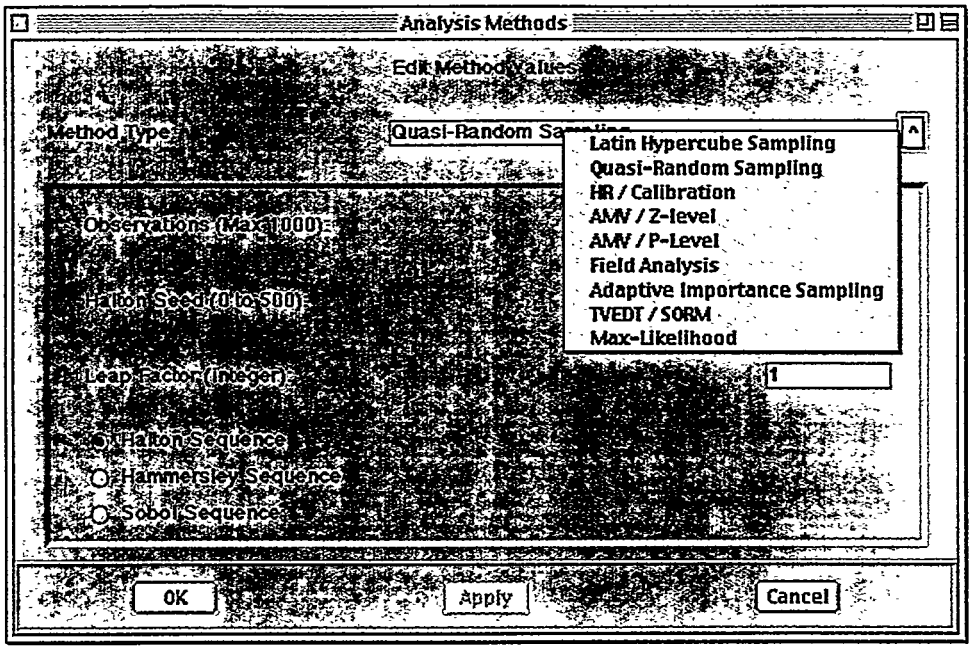

Figure 5.4 Analysis Method Options

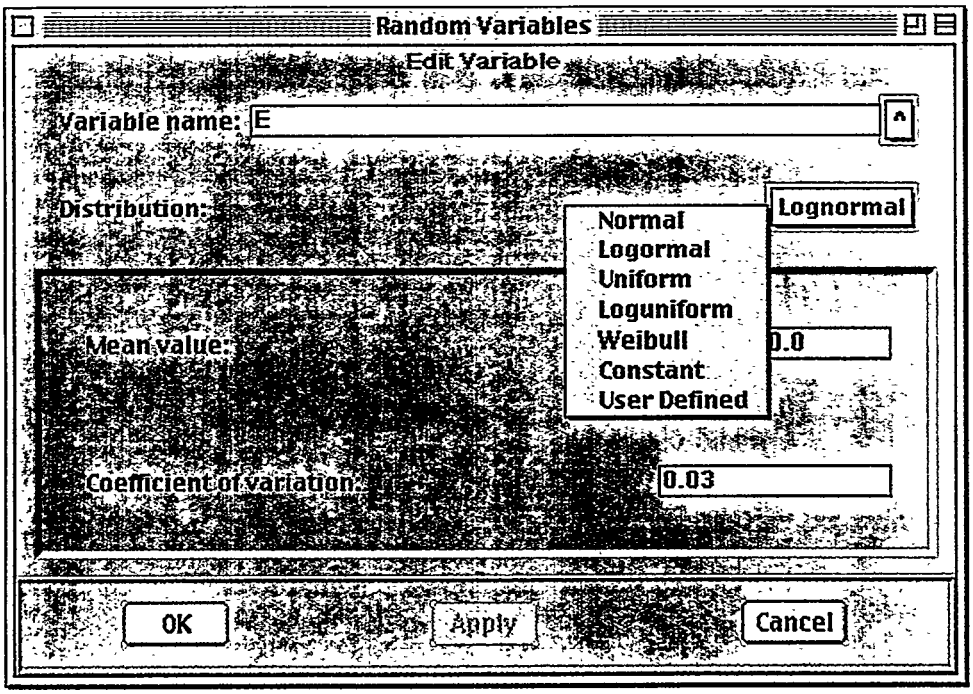

Figure 5.5 Distribution Selection

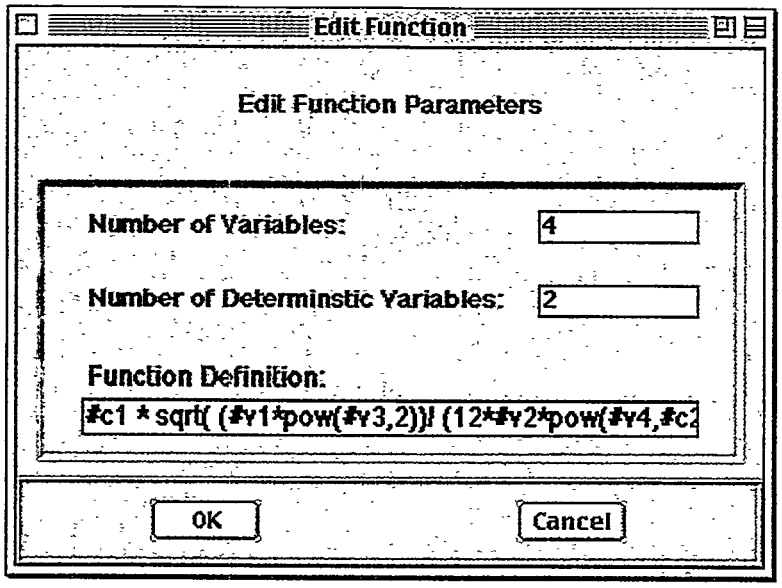

Figure 5.6 Generic Function Input Option

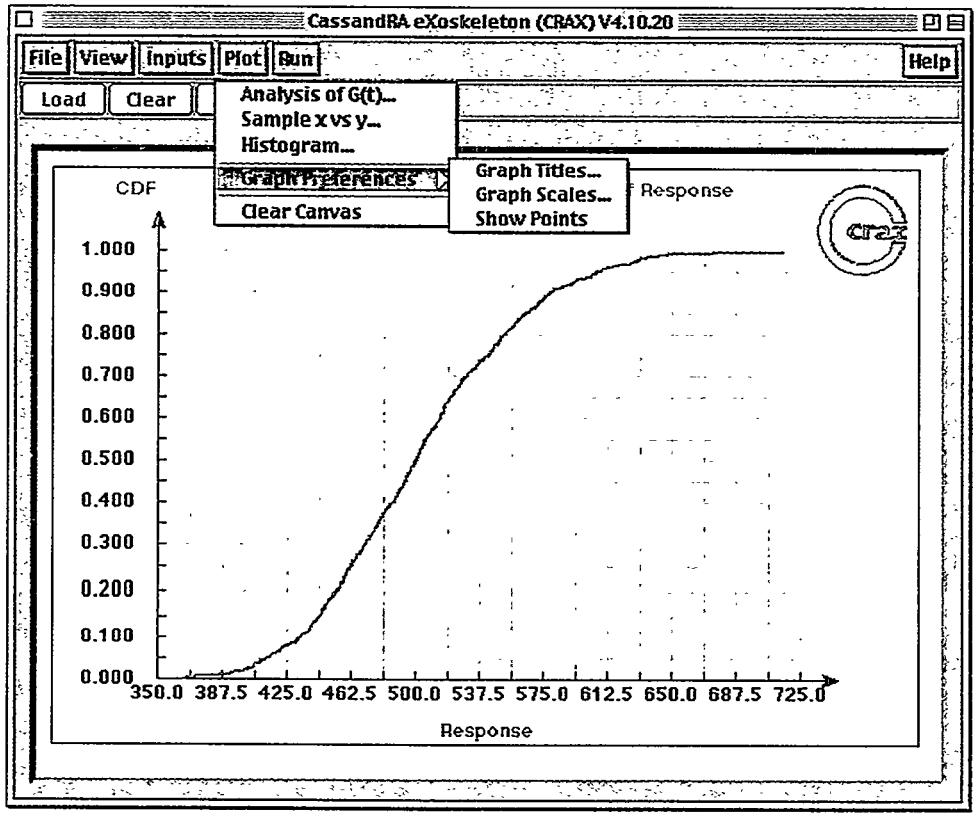

Figure 5.7 Plotting Options

Output is done primarily through a graphical depiction of the cumulative distribution, probability density function and sensitivity analysis (e.g. Figure 5.8). Pairwise plots of the sample deviates is also available. (The exact options are a function of the analysis method chosen.). The axes

scales and titles are input by the user along with the title for the overall graph. As mentioned previously the user can save the graph as an encapsulated postscript file for later use.

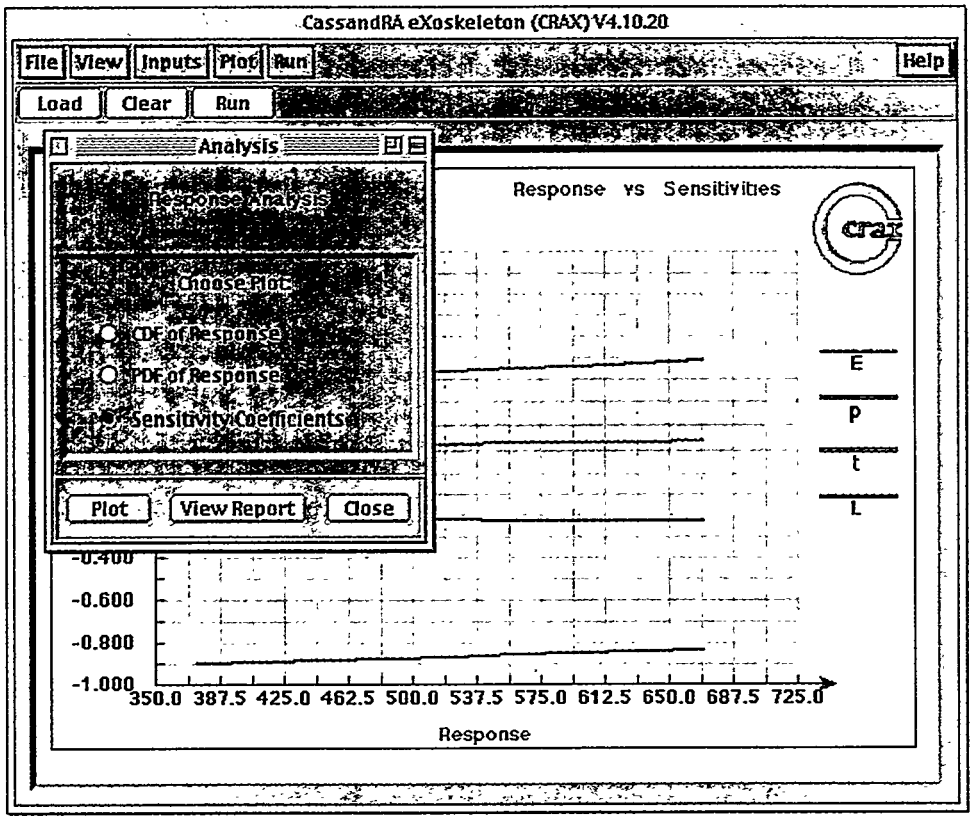

Figure 5.8 Sensitivity Analysis

5.5 Software Accessibility

The exchange of information between the CRAX GUI, Cassandra, and the physical model can take many forms. Within CRAX is the capability to either recompile the existing software into the Cassandra engine, thereby significantly increasing computational efficiency, or rely on 'hand-shaking' between the CRAX GUI, the Cassandra engine and the existing software. The Tcl/Tk interface can be modified to handle either of these situations very easily. In addition, Cassandra is platform independent and complies with the Common Object Request Broker Architecture (CORBA) permitting easy interface with many of the new engineering design and analysis software packages (Figure 5.9). Over 400 commercial software vendors have adopted the CORBA interface standards, e.g. Hewlett-Packard.

In addition, the use of the CORBA interface permits the easy integration of reliability and uncertainty methods into the Product Realization Environment (PRE) at Sandia. The PRE framework has been designed and developed in support of Sandia National Laboratories Product Realization backbone with the goal of providing new and improved information tools to help reduce the time and cost for realizing nuclear weapons components.

The use of a standard interface architecture also permits the easy integration of the uncertainty methods in Cassandra and the routines in the comprehensive optimization package being developed at Sandia (DAKOTA). (It should be noted that there is a 'generic' version of

CRAX/Cassandra in which the user types in their own performance function directly into the CRAX interface.)

5.6 Summary

The CRAX/Cassandra reliability analysis software is constantly being updated as additional existing reliability analysis methods are incorporated into Cassandra and new analysis techniques are developed. Each new design problem brings with it a unique set of input, output and computational requirements. The flexibility of the CRAX interface and the extensibility of the Cassandra uncertainty engine permits the reliability issues to be addressed quickly and efficiently whatever the computational requirements might be. The software continues to provide new insights into issues related to stockpile surveillance that were not possible before.

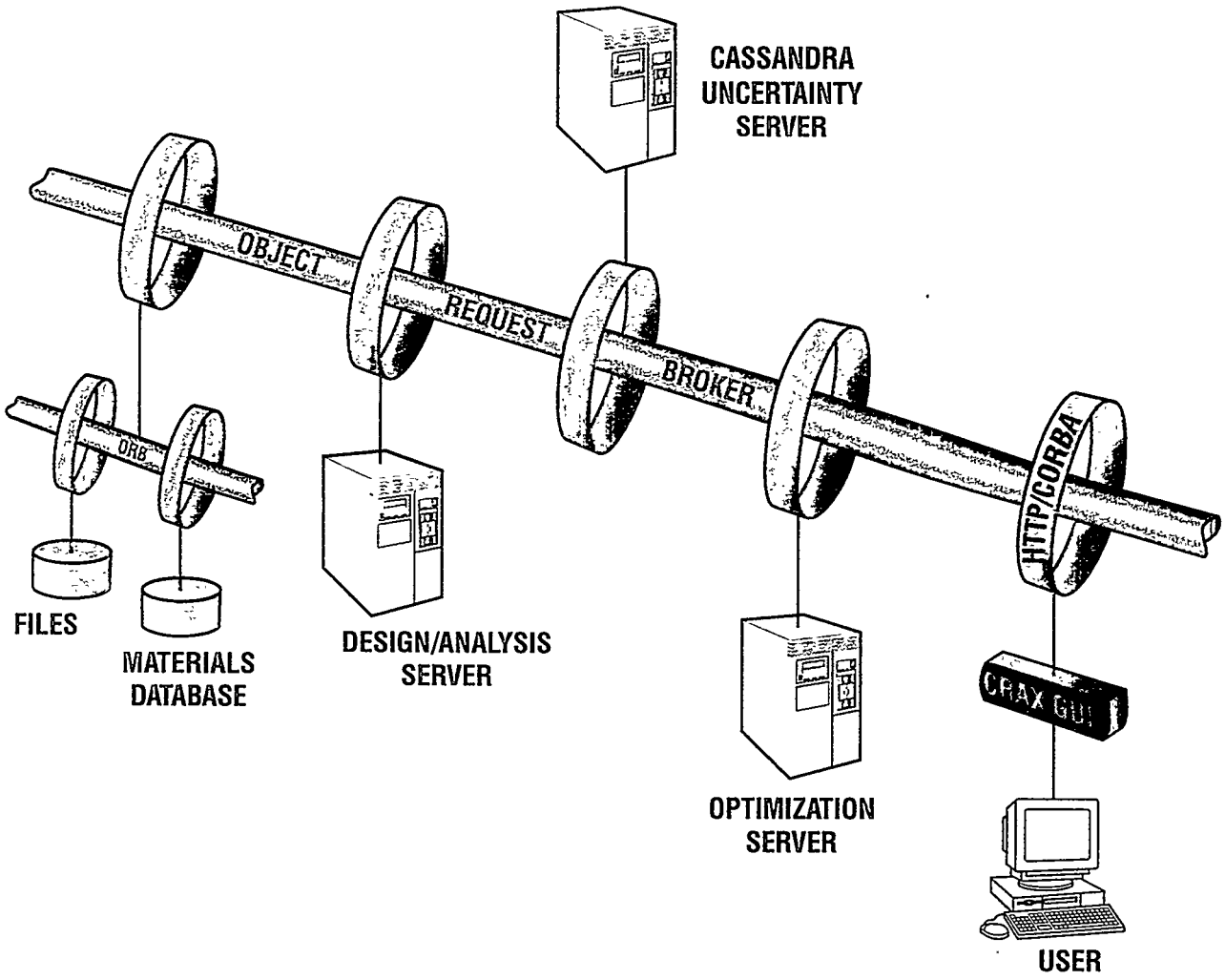

Figure 5.9 Network Accessibility

6.0 References

Breitung, K., 1984, Asymptotic Approximation for Multinormal Integrals, *Journal of Engineering Mechanics*, ASCE, Vol. 110, No. 3, pp. 357-366

Engelmaier, W., 1991, "Solder Attachment Reliability, Accelerated Testing, and Result Evaluation," Solder Joint Reliability: Theory and Applications, J. H. Lau editor, Ch. 17, pp545-587.

Hohenbichler, M., R. Rackwitz, 1981, "Non-Normal Dependent Vectors in Structural Safety," *Journal of the Engineering Mechanics Division*, ASCE, Vol. 107, No. EM6, December, pp1227-1238.

Korhonen, M, 1993, "Microstructure Based Statistical Model of Electromigration Damage In Confined Line Metalizations in the Presence of Thermally Induced Stresses," Journal of Applied Physics, Vol. 74, No. 8, October, pp4995-5004.

Robinson, D., 1998, "A Survey of Probabilistic Methods Used in Reliability, Risk and Uncertainty Analysis: Analytical Techniques I," SAND98-1189, Sandia National Laboratories, Albuquerque, New Mexico, June.

Robinson, D., C. Atcitty, 1999, "Comparison of Quasi- and Pseudo-Monte Carlo Sampling for Reliability and Uncertainty Analysis," AIAA Structures, Structural Dynamics and Materials Conference, St. Louis, MO, 12-15 April.

Shinozuka, M., 1983, "Basis Analysis of Structural Safety,", Journal of Structural Division, ASCE, Vol. 3, No. 109, March.

Yost, F.G., D. E. Amos, A. D. Romig, Jr., 1989, "Stress-Driven Diffusive Voiding of Aluminum Conductor Lines," *Proceedings of the International Reliability Physics Symposium*, pp. 193-201

Yost, F. G., 1989, "Voiding Due to Thermal Stress in Narrow Conductor Lines," Scripta METALLURGICA, Vol. 23, pp. 1323-1328.

Yost, F. G., A. D. Romig, Jr., R. J. Bourcier, 1989, "Stress Driven Diffusive Voiding of Aluminum Conductor Lines," *Diffusion Analysis & Applications*, pp273-288

Yost, F. G., F. E. Campbell, 1990, "Stress-Voiding of Narrow Conductor Lines," *Circuits and Devices*, May , pp40-44

Distribution

1	MS 1407	(1805) R. J. Salzbrenner	
1	MS 1407	(1811) K. Gillen	
1	MS 0340	(1832) J. W. Braithwaite	
1	MS 0340	(1832) N. R. Sorensen	
1	MS 1411	(1833) F. M. Hosking	
1	MS 1411	(1833) P. T. Vianco	
1	MS 1411	(1834) F. G. Yost	
1	MS 0746	(6411) R. M. Cranwell	
1	MS 0747	(6412) A. L. Camp	
1	MS0748	(6413) J. H. Lee	
1	MS 0746	(6411) D. J. Anderson	
1	MS 0746	(6411) L. A. Painton-Swiler	
10	MS 0746	(6411) D. G. Robinson	
1	MS 0747	(6412) G. D. Wyss	
1	MS 9102	(8402) M. W. Perra	
1	MS 0819	(9231) T. G. Trucano	
1	MS 0439	(9234) D. R. Martinez	
1	MS 0439	(9234) J. R. Red-Horse	
1	MS 0439	(9234) M. S. Eldred	
1	MS 0829	(12323) K. V. Diegert	
1	MS 0829	(12323) B. M. Rutherford	
1	MS 0830	(12335) J. M. Sjulin	
1	MS 0188	LDRD office	D. L. Chavez
1	MS 9018	(8940-2)	Central Technical Files
2	MS 0899	(4916)	Technical Library
1	MS 0619	(00111) DOE/OSTI	Review & Approval Desk for

TOTAL COPIES = 36